SUPERCONDUCTING TUNNEL DIODES

INVESTIGATIONS ON
ASYMMETRICAL AND SYMMETRICAL
SUPERCONDUCTING THIN-FILM TUNNEL JUNCTIONS

By

RAO V. V. N. SIMHA

A Thesis
Submitted to the Faculty of Graduate Studies
in Partial Fulfilment of the Requirements
for the Degree
Master of Engineering

McMaster University
April 1967

MASTER OF ENGINEERING | McMASTER UNIVERSITY

(Electrical Engineering) | Hamilton, Ontario

TITLE: Investigations on Asymmetrical and Symmetrical Superconducting Thin-Film Tunnel Junctions

AUTHOR: Rao V. V. N. Simha, M.Sc. (Andhra University, India)

SUPERVISOR: Professor C. K. Campbell

NUMBER OF PAGES: v, 68

SCOPE AND CONTENTS:

This thesis is concerned with the phenomenon of electron tunneling between thin-film superconductors. The tunneling equations are investigated and applied, in particular, to an experimental study of tin/insulator/lead structures.

As an aid to further possible analysis of the basic properties of superconductors, circuits are also examined which directly yield the dI/dV and d^2I/dV^2 characteristics of symmetrical tunneling fabrications, such as lead/insulator/lead junctions.

Finally, a brief study is made of the feasibility of several circuits which employ the tin/insulator/lead type asymmetrical tunneling junctions as active elements.

ACKNOWLEDGEMENTS

I am thankful to the fatherly treatment and constant encouragement of my Supervisor, Dr. C. K. Campbell, and to the help and co-operation of my Senior in the Low Temperature Laboratory, Mr. R. C. Dynes.

I greatly owe to all my colleague graduate students, who made my stay at McMaster interesting, my sincere thanks.

Finally, I thank Miss M. Kaneary for typing this thesis.

CONTENTS

CHAPTER 1

INTRODUCTION

1.1 Historical Sketch

Superconductivity, one of the most unusual physical phenomena, is attracting particular attention at present. The construction of powerful electromagnets from superconducting alloys, and giving fields up to 100 KOe., led to a substantial increase in the pace of scientific and technological research on the subject. In addition, the application of the cross-film cryotron to digital circuits and storage elements has initiated a detailed study of this phenomenon.

The historical developments and the present state of the theory of superconductivity are reviewed very recently by Abrikosov[1]. Some of the features are presented in this introductory section.

Superconductivity was discovered by the Dutch physicist Kamerling-Onnes[2] in 1911. He measured the electric resistivity of metals at liquid helium temperatures and found that at a temperature near $4^{o}K$ the resistance of mercury suddenly drops to zero. Subsequently many more superconducting metals and alloys were discovered with widely differing values of transition temperatures, or so-called critical temperature, T_{cr}, $18^{o}K$ is that of the alloy Nb_3Sn, while the alloy Bi_2Pt, for example, has a critical temperature of only $0.155^{o}K$.

In 1914 Kamerlingh-Onnes discovered that superconductivity is destroyed when the metal is placed in a sufficiently strong magnetic field[3], H_{cr} (critical field). The magnitude of this critical field is a temperature dependent function. It is greatest at absolute zero and decreases with rising temperature to become zero at the critical temperature. If the transition takes place in the presence of a magnetic field it is a normal phase transition, a so-called first order transition, which is accompanied by the release or absorption of a latent heat. If the transition takes place in the absence of a magnetic field, i.e., at T_{cr}, it is a transition of second order, in which there is no latent heat. Silsbee[4] later showed that superconductivity is destroyed by the passage of an electric current exceeding a certain magnitude.

Another important property of superconductors was discovered in 1933 by Meissner and Ochenfeld[5]. It was found that an external magnetic field does not penetrate into the body of a thick superconductor, and that on the transition into the superconducting state the field is, as it were, pushed out of the superconductor. It was shown theoretically by Mrs. de Haas[6] in 1931, and experimentally by Shoenberg[7] in 1940, that this is connected with the appearance of currents in a surface layer of the superconductor of 10^{-5}- 10^{-6} cm. thickness which screen the interior of the superconductor from the external field. The thickness of this layer is called the "penetration depth".

Subsequent to these initial experiments, research on this phenomenon was carried out by a number of investigators[8-14]. The basic cause of superconductivity remained a mystery, however, until the 1950's.

In 1950 Reynolds et al[15], working with mercury and Maxwell[16], working on tin, discovered an interesting phenomenon: The influence of the isotopic composition of the metal on its critical temperature.

In addition to the electrons, the metal contains positively charged ions, which form the crystal lattice. A change in isotopic composition means a change in the mass of the ions. The latter, however, influence only the vibrational frequencies of the lattice. It was deduced, therefore, that the lattice vibrations were directly connected with superconductivity. Starting from this discovery, Fröhlich[17] and Bardeen[18] developed a theory of a particular kind of attraction between the electrons. One of the consequences of quantum mechanics is the conclusion that a lattice must always, even at absolute zero, be in a vibrating state (zero-point vibrations). According to the theory of Fröhlich and Bardeen each electron changes the behaviour of the zero-point vibrations and this gives rise to a field of force which acts on another electron. In this way there must be an interaction between the electrons which is necessarily attractive and can dominate over the electrostatic repulsion.

On the basis of this fact Bardeen, Cooper and Schrieffer[19] (often referred as BCS) developed a microscopic theory of superconductivity which gave a fairly complete explanation of the phenomenon.

It was shown that the attractive forces lead to the formation of bound pairs (sometines called Cooper pairs). It is interesting that this is not just a process involving the two electrons which form the pair, but that the whole collective system of electrons in the metal take part. It turns out in particular that for this reason, an arbitrary weak attraction is sufficient for the formation of pairs. Any transfer of energy to the electron fluid in the superconductor requires the breaking of a pair. But this means that the energy which is transferred cannot be arbitrarily small, but must necessarily exceed the binding energy of a pair. This lower limit to the energy transfer is called the "gap" in the electron energy spectrum. From the existence of an energy gap it follows that a fluid of electron pairs can move without friction, up to a certain velocity. In other words an electric current flows without resistance. As already been stated, the pair formation is a collective effect and is therefore connected with the state of the whole electron system. As the temperature is increased, some of the pairs are broken, and this in turn affects the binding energy of the remaining pairs. As a result, the binding energy decreases, and at the critical temperature it becomes zero. No pairs are left and the metal becomes normal in all respects.

1.2 Some Equations of the Superconductive State

Some well-established equations, which describe some properties of superconductive state are presented in this section.

(1) Energy Gap:

The binding energy of a pair is $2\Delta(T)$ at temperature $T^{o}K$; and that at absolute zero is $2\Delta(0)$.

$$\Delta(0) = 2\hbar\, \omega_D e^{-1/\eta} \qquad 1.1$$

where $\hbar = h/2\pi$, h is the Plank's constant and ω_D is the Debye frequency. The quantity η is a dimensionless constant which measures the interaction of the electrons with the lattice. In all known cases $\eta<\frac{1}{2}$.

The temperature dependence of the energy gap is determined by numerical solution of the integral

$$\frac{1}{\eta} = \int_0^{t\omega_D} \frac{\tan\ (\varepsilon/2kT)}{2\varepsilon}\ dE \qquad 1.2$$

where $\varepsilon = |E^2 + \Delta^2(T)|^{1/2}$, E is the electron energy.

A rather useful result is found by combining equation 1.1 and 1.2, namely:

$$2\Delta(0) = 3.52\ kT_{cr} \qquad 1.3$$

(2) Critical Temperature:

The critical temperature T_{cr} in energy units is given by:

$$T_{cr} = \Delta(0)/1.76 \qquad 1.4$$

It is possible that the smallness of the critical temperature is connected with the existence of a limit for η.

(3) Electronic Specific Heat:

(a) In normal State:-

$$C_n = \gamma T$$

where C_n is the electronic specific heat of the metal in the normal state and γ is a coefficient having a value $10^2 - 10^4$ erg/cm^3. deg.^{2}.

(b) Near T = 0

$$\frac{C_s(T)}{C_n(T_{cr})} = 1.35 \left(\frac{\Delta(0)}{T}\right)^{3/2} e^{-\Delta(0)/T} \qquad 1.6$$

where $C_s(T)$ is the specific heat due to superconducting electrons and $C_n(T)$ is the specific heat of the normal metal at the critical temperature.

(c) Near $T = T_{cr}$

$$\frac{C_s(T)}{C_n(T_{cr})} = 2.42 + 3.77\left(\frac{T}{T_{cr}} - 1\right) \qquad 1.7$$

from which we see that the specific heat has a discontinuity at $T = T_{cr}$.

(4) Critical Field:

(a) Near T = 0

$$H_{cr}(T) = H_{cr}(0) \left[1 - 1.06 \left(\frac{T}{T_{cr}}\right)\right]^2 \qquad 1.8$$

where $H_{cr}(T)$ is the critical field for $T<T_{cr}$, which when applied to the superconductor, brings it back to the normal state and $H_{cr}(0)$ is the critical field at absolute zero. $H_{cr}(0)$ is proportional to T_{cr} and may be in the region of hundreds to thousands of Oersted.

(b) Near $T = T_{cr}$

$$H_{cr}(T) = 1.73\ H_{cr}(0) \left(1 - \frac{T}{T_{cr}}\right) \qquad 1.9$$

(5) Density-of-States:

As pointed out earlier, in addition to the electrons, the metal contains positively charged ions which form the crystal lattice. An electron moving through a lattice causes a localized polarization of the ionic structure which may be described as a cloud of virtual phonons. Emission and reabsorption of these virtual phonons is a dynamic process taking place all the time in a normal metal; it introduces the need for renormalization of the electron mass and gives rise to the concept of a quasi-particle. The BCS theory takes into account a process involving pairs of electrons which interact through the exchange of a virtual phonon. This theory gives the following expression for the density-of-states function, $\rho_s(E)$, for the excited quasi-particle of the superconductor.

$$\left.\begin{aligned} \rho_s(E) &= \rho_n(E)\left[\frac{E}{\{E^2 - \Delta^2(T)\}^{\frac{1}{2}}}\right], \qquad |E| \geq \Delta(T) \\ \rho_s(E) &= 0 \qquad\qquad\qquad\qquad\qquad\quad, \qquad |E| < \Delta(T) \end{aligned}\right\} \qquad 1.10$$

where $\rho_n(E)$ is the density-of-states function at the Fermi-level in the normal state and E is the energy level.

1.3 Tunneling Between Superconductors

(A) Qualitative Expanation:

The superconducting tunnel-junction, which normally consists of a system of two superconductors, or a superconductor and a normal metal separated by a very thin layer of dielectric of a few atomic distances thickness, has received considerable theoretical and experimental investigations. It was discovered by Giaever[20] in 1960, giving a non-linear current-voltage characteristic for a normal-superconductor junction. Later it was reported that if the two metals constituting the junction were different and are superconducting, the current-voltage characteristic of the junction exhibited a negative-resistance pattern[21,22]. The metals are usually vacuum deposited and the dielectric provided by a thermally-grown oxide film on the bottom metal film.

This simple device has turned out to be an extremely valuable tool for studying the nature of superconductivity. From the variation of the current through the junction with the applied potential difference across it, one can deduce the binding energy of the pairs, its temperature dependence and its anisotropy in a single crystal. One can also determine the singularities in the spectrum of lattice vibrations.

The mechanism for current flow from one superconductor to the other through the insulating layer, as in the semiconductor tunnel diode, is quantum-mechanical electron tunneling. In the following discussion we shall consider only the low-voltage region, where the current flowing through the insulating film is proportional to the voltage across it, provided both metals are in normal state and thus the I-V relationship is an ohmic one. The dependence of tunneling current on applied voltage changes strongly if one or both metals become superconducting.

The main purpose of this thesis is to investigate the tunneling properties of tin-lead and lead-lead junctions and the possible circuit applications of the former type of junction. The present section briefly explains some of the tunneling phenomena in terms of the "BCS model", together with the "semiconductor analogy".

To examine tunneling characteristics of a metal junction, it is helpful to consider the LHS diagrams of Figure 1.1, which represent the density-of-state curves of the metals. Note how the curves have changed in the superconducting state, leaving an energy gap centered at the Fermi-level, as pointed out in Section 1.2. If an external potential is applied across the two metals, the Fermi-levels are shifted with respect to one another.

If the two metals are in the normal state as in Figure 1.1 (a), the shift between the Fermi-levels causes a tunnel current flow and it is found experimentally that this current varies linearly with the applied potential, if this potential does not exceed a few millivolts.

In Figure 1.1(b) is shown the case when one of the two metals is in superconducting state. Most of the Fermi electrons of the normal

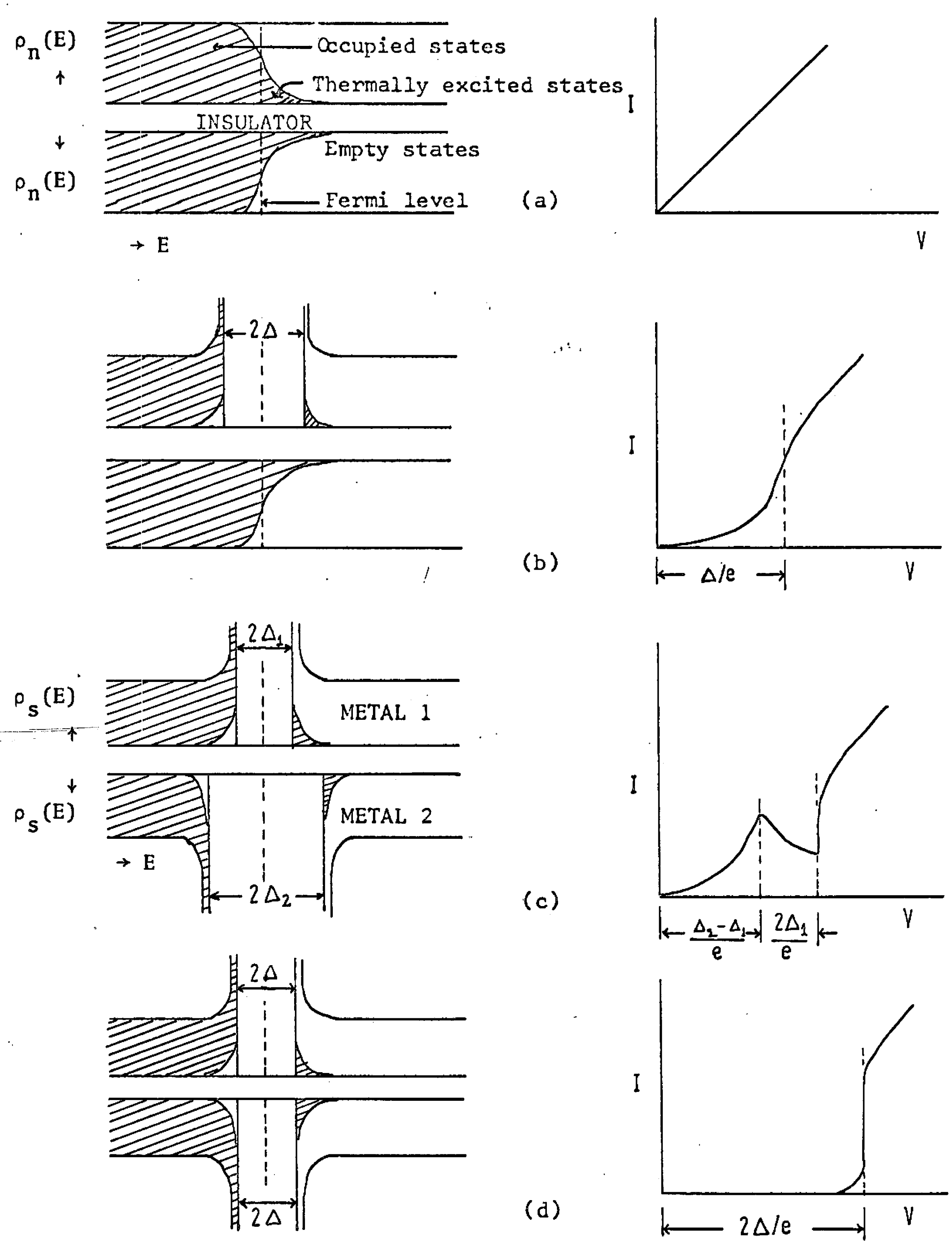

Figure 1.1 Density-of-states and I-V Characteristics

metal are now seen to be opposite the forbidden energy region of the superconductor. It is clear that the potential across the junctions must be raised to Δ/e (corresponding to the half of the energy gap) in either a positive or negative sense before a significant tunneling current can flow. At first, there is a very rapid rise of current with voltage due to the large density of piled-up stages; for voltages exceeding Δ/e, the tunneling samples the density-of-states well beyond the gap and I-V curve approaches the purely ohmic character of N-N case.

Figure 1.1(c) can be used to analyze tunneling between two superconductors having widely different energy gaps. If a potential is applied that lowers the energy of the electrons of Metal-2 (having the larger energy gap $2\Delta_2$), some of the electrons which are thermally excited across the gap of Metal-1 will now be able to tunnel to the empty states just on the RHS of the energy gap of Metal-2. This leads to the first increase in the tunnel current, shown at the potential $(\Delta_2 - \Delta_1)/e$. However, as the potential across the junction is increased further, the tunnel current decreases, due to the decrease in the density of available states in Metal-2. This produces the region of negative slope in the I-V characteristic. Finally, as the potential is increased to $(\Delta_2 + \Delta_1)/e$ the main body of unexcited electrons in Metal-1 is brought opposite the empty states of Metal-2, thus leading to the major current increase shown in the RHS curve of Figure 1.1(c).

If the two superconductors have equal energy gaps, the negative-conductance region is strongly reduced, so that a rectangular curve similar to that shown schematically in Figure 1.1(d) results.

(B) <u>Quantitative Analysis:</u>

Figure 1.3(c) may be used to derive the qualitative relations for the tunneling currents for the various cases described above. The following conventions are adopted that a) positive voltages are applied to Metal-1 and b) changes in spectral energy are relative, with metal-1 fixed as reference in the pictorial representation.

For this one-dimensional model, the one-way tunneling current is proportional to an integral, over all energies, of the product of the number of occupied states in one metal at a given energy level times the number of unoccupied states (holes) in the other metal at the corresponding energy, multiplied by the probability for an electron to go through the barrier at constant energy[23]. The net current is given by the difference in the opposed one-way currents. It is convenient to consider the zero-energy level to be at the Fermi-level for Metal-1, E_{f1}, and to express all energies in units of kT. Then

$$I \alpha \int_{-\infty}^{\infty} \left[\rho_2(E-V) f(E-V) \rho_1(E)\{1-f(E)\} P_{2\to1} - \rho_2(E-V)\{1-f(E-V)\} \rho_1(E) f(E) P_{1\to2}\right] dE \qquad 1.11$$

where V is the energy equivalent of the applied voltage, ρ_1 and ρ_2 are the density-of-states, $P_{2\to1}$ and $P_{1\to2}$ are the probabilities of an electron tunneling from Metal-2 to Metal-1 and vice-versa, and f(E) is the Fermi-function given by 1/(1 + expE).

Because of the action of the Fermi-functions, the important region of integration is confined to an interval of a few kT about the Fermi-level. With the assumption that the tunneling probability is constant over this energy interval and that $P_{2\to1}$ is equal to $P_{1\to2}$. Equation 1.11 reduces to:

$$I = \text{const} \times \int_{-\infty}^{\infty} \rho_2(E-V)\rho_1(E)\,|f(E-V)-f(E)|\, dE \qquad 1.12$$

$\rho_1(E)$ and $\rho_2(E)$ are represented by $\rho_s(E)$ or $\rho_n(E)$ depending upon whether the particular metal is in the superconducting or normal state. Further, becuase of the slowly-varying nature of $\rho_n(E)$ in the vicinity of the Fermi-level, it shall be taken as constant for both metals, and $\rho_s(E)$ is given by Equation 1.10. It is now convenient to combine these constants into the proportionality constant and to use a system of current units such that the total constant has a value of unity.

Different cases of interest are treated in detail by Shapiro, et al[24], based on the above analysis. The final expressions derived for machine computation are summarized here.

CASE I: One metal superconducting

On substitution of the expressions for the density-of-states functions and the Fermi functions, the current is given by:

$$I = \int_{-\infty}^{\infty} \frac{E - V}{\left[(E-V)^2 - \Delta^2\right]^{\frac{1}{2}}} \cdot \frac{\exp E\,\left[1-\exp\,(-V)\right]}{\left[1-\exp\,(E-V)\right]\left[1 + \exp E\right]}\, dE \qquad 1.13$$

Since the first term of the integrand is discontinuous at $E = V \pm \Delta$, the range of integration must be subdivided at these points. Let I be equal to $I_1 + I_2$. Further, if the following substitutions

$$\left.\begin{aligned} E &= V - (u^2 + \Delta^2)^{\frac{1}{2}}, &\quad \text{in } I_1 \\ E &= V + (u^2 + \Delta^2)^{\frac{1}{2}}, &\quad \text{in } I_2 \end{aligned}\right\} \qquad 1.14$$

are made, the individual currents are given by

$$\left.\begin{aligned} I_1 &= \int_0^{\infty} \frac{\exp V - 1}{\left[1 + \exp(u^2 + \Delta^2)^{\frac{1}{2}}\right]\left[1 + \exp\{V - (u^2 + \Delta^2)^{\frac{1}{2}}\}\right]}\, du \\ I_2 &= \int_0^{\infty} \frac{\exp V - 1}{\left[1 + \exp\{-(u^2 + \Delta^2)^{\frac{1}{2}}\}\right]\left[1 + \exp\{V + (u^2 + \Delta^2)^{\frac{1}{2}}\}\right]}\, du \end{aligned}\right\} \qquad 1.15$$

CASE II: Both metals superconducting.

A similar substitution as in Case I gives the current as:

$$I = \int_{-\infty}^{\infty} \frac{E}{\left[E^2 - \Delta_1^2\right]^{\frac{1}{2}}} \cdot \frac{E - V}{\left[(E-V)^2 - \Delta_2^2\right]^{\frac{1}{2}}} \cdot \frac{\exp E \left[1 - \exp(-V)\right]}{\left[1 + \exp(E - V)\right]\left[1 + \exp E\right]} \, dE \qquad 1.16$$

Singular points may occur at $E = \pm \Delta, V \pm \Delta_2$. Some of these singular points may be suppressed for certain ranges of voltages and at particular values of V, certain of these may coincide. Without a loss of generality it may be assumed that $\Delta_1 \leqslant \Delta_2$.

It is now clear that three ranges of V must be investigated, namely:

$$\left.\begin{array}{ll} I = I_1 + I_2 , & 0 < V < \Delta_2 - \Delta_1 \\ I = I_2 + I_3 , & \Delta_2 - \Delta_1 < V < \Delta_2 + \Delta_1 \\ I = I_2 + I_3 + I_4 , & \Delta_2 + \Delta_1 < V \end{array}\right\} \qquad 1.17$$

The individual currents on eliminating the singularities can be shown to be given by:

$$\left.\begin{array}{l} I_1 = \displaystyle\int_0^{\infty} \frac{E\,(E + V)}{(E + {}_1)(E + V + {}_2)^{\frac{1}{2}}} \cdot \frac{\exp(-E)\left[1 - \exp(-V)\right]}{\left[1 + \exp\{-(E+V)\}\right]\left[1 + \exp(-E)\right]} \, du \\ \text{where} \quad E = \frac{1}{2}(\Delta_2 - \Delta_1 - V)\cosh(u) + \frac{1}{2}(\Delta_2 + \Delta_1 - V) \end{array}\right\} \qquad 1.18$$

$$\left.\begin{array}{l} I_2 = \displaystyle\int_0^{\infty} \frac{E(E - V)}{\left[(E + \Delta_1)(E - V + \Delta_2)\right]^{\frac{1}{2}}} \cdot \frac{\exp E \left[1 - \exp(-V)\right]}{\left[1 + \exp(E-V)\right]\left[1 + \exp E\right]} \, du \\ \text{where} \quad E = \frac{1}{2}(\Delta_2 - \Delta_1 + V)\cosh(u) + \frac{1}{2}(\Delta_2 + \Delta_1 + V) \end{array}\right\} \qquad 1.19$$

$$I_3 = \int_0^{\infty} \frac{E\,(E + V)}{\left[(E + \Delta_1)(E + V + \Delta_2)\right]^{\frac{1}{2}}} \cdot \frac{\exp(-E)\left[1 - \exp(-V)\right]}{\left[1 + \exp\{-(E+V)\}\right]\left[1 + \exp(-E)\right]}\,du$$

where $E = -\frac{1}{2}(\Delta_2 - \Delta_1 - V)\cosh(u) + \frac{1}{2}(\Delta_2 + \Delta_1 - V)$ (1.20)

$$I_4 = \int_{-\pi/2}^{\pi/2} \frac{E\,(V - E)}{\left[(E+\Delta_1)(V-E+\Delta_2)\right]^{\frac{1}{2}}} \cdot \frac{\exp E\left[1 - \exp(-V)\right]}{\left[1 + \exp(E-V)\right]\left[1 + \exp E\right]}\,du$$

where $E = \frac{1}{2}(V - \Delta_1 - \Delta_2)\sin(u) + \frac{1}{2}(V + \Delta_1 - \Delta_2)$ (1.21)

The integrals of Equations 1.15 and 1.18 through 1.21 have been evaluated numerically on a digital computer (IBM 7040), and are presented in Chapter 3 for comparison with the experimental plots. In Equations 1.18, 1.19 and 1.20 the integrands behave as exp (-cosh U) and hence the numerical integration process can safely be terminated as soon as the integrand is negligible.

Note that in I_1 the value of E is constant when $V = \Delta_2 - \Delta_1$. Since the range of integration is unlimited, the value of I_1 will be infinite. The mathematical singularity is due to using the strict BCS form for the density-of-states, which itself has a singularity. For a real system the density-of-states would be rounded-off[25].

The integrand of I_4 is likewise a constant when $V = \Delta_1 + \Delta_2$. Since the range of integration is finite in this case, the analysis predicts a discontinuity in the graph of the current at $V = \Delta_1 + \Delta_2$ and also that the height of the current jump will be proportional to the value of I_4 at this value. Again for a real system, one consequence of the rounding-off parameter could be to spread the current jump over a small region of voltage about the value $V = \Delta_1 + \Delta_2$.

(C) Density-of-States and Phonon Spectra from Derivative Plots:

It may be noticed from the previous sections that the central part in the BCS theory is the creation of an energy gap in the electron density-of-states when a metal is made superconducting. By using the tunneling techniques one obtains not only the magnitude of the energy gap, but also the corresponding density-of-states and phonon spectra.

For $T > 1^{\circ}K$, kT is still an appreciable fraction of the energy gap and results in a temperature smearing. To overcome this and to give a closer check to the BCS theory Giaever, Hart and Megerle[26] devised a method of measuring the slope of the I-V curve (dV/dI or the dynamic resistance) directly, as it is this resistance which is inversely proportional to the density-of-states. Experimenting with different metals they observed a striking resemblance for density-of-states with theory, except for the two bumps in the case of lead at higher energies of approximately 2Eg and 4Eg, Eg being the full energy gap. They have accounted for these bumps by introducing an energy-gap parameter Δ_k which is not constant.

Rowell, Chynoweth and Phillips[27] have reported further structure in the tunneling characteristic. The positions of the several humps were more easily taken as peaks from d^2I/dV^2 versus V plots, which further resolved several more at higher biases. Considerable refinement in experimental technique has allowed Rowell, Anderson and Thomas[28] and Rowell and Kopf[29] to report many developments.

(a) The density-of-states variation suggests the form of the phonon spectrum which is effective in the coupling of Cooper pairs. The location of transverse and longitudinal acoustical phonon frequencies from the second derivative plot is very straight forward.

(b) A solution of the Eliashberg gap equation[30] using such phonon spectrum and reasonable values for coupling constants gives good agreement between theoretical and experimental density-of-states plots, as shown by Schrieffer, et al[31].

(c) The structure is resolved in detail and much of it can be assigned to specific Van Hove[32] singularities.

(d) It is also determined how far the phonon spectrum extends in even weakly-coupled superconductors such as tin, indium, etc.

The refinements and design details of second harmonic detection have been reported by Thomas and Rowell[33]. A similar technique, but with a tuned amplifier instead of an impedance transformation reactance network and an amplifier has been used by Walmsley[34] in investigating the anisotropy in superconductive tunneling and by Dynes[35] in studying the changes in phonon spectrum of lead with impurities such as bismuth. The general layout of such a system is presented in Section 2.5 and Section 2.6 describing the design details of the 1 KHz tuned amplifier. This amplifier, which forms a part of the present project, is constructed to achieve low-noise, low-level signal performance. The derivative characteristics thus obtained are included in Section 3.2.

CHAPTER 2

EQUIPMENT, FABRICATION AND ELECTRONIC CIRCUITRY

2.1 Vacuum Coating Unit

An Edward model 12E3, multi-filament vacuum-coating unit is utilized to fabricate the thin-film tunneling junctions for the experiments described in the following chapters. The coating unit has an oil-diffusion-pump and rotary-pump combination capable of attaining pressure below 10^{-7} torr. In practice, however, leaks and bell-jar contamination limit the vacuum attained to about 2×10^{-6} torr. The rotary-pump starts pumping at atmospheric pressure and reduces the pressure to 2×10^{-4} torr. This pressure is much too high to allow uncontaminated evaporation of most film; hence, the need for a diffusion-pump to reduce the pressure further.

A liquid nitrogen trap in the form of a spirally wound copper tubing, fed from a pressurized liquid-nitrogen dewar, is built in the unit, between the diffusion-pump and the bell-jar, to prevent the back flow of the diffusion-pump oil into the evaporator and to condense water and other vapours present. A similar trap is provided on the top of the subtrate mount.

2.2 Cryostat and Sample Holder

The cryostat used is as shown in Figure 2.1. This cryostat allows the immersion of the sample under study directly into the liquid

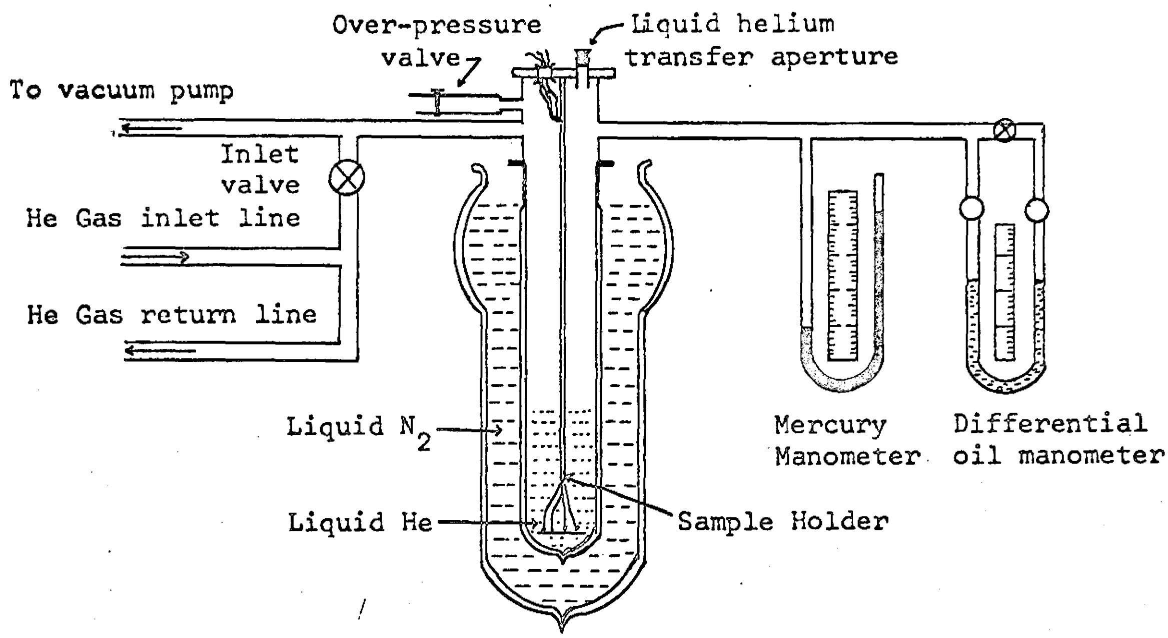

Figure 2.1 Cryostat assembly

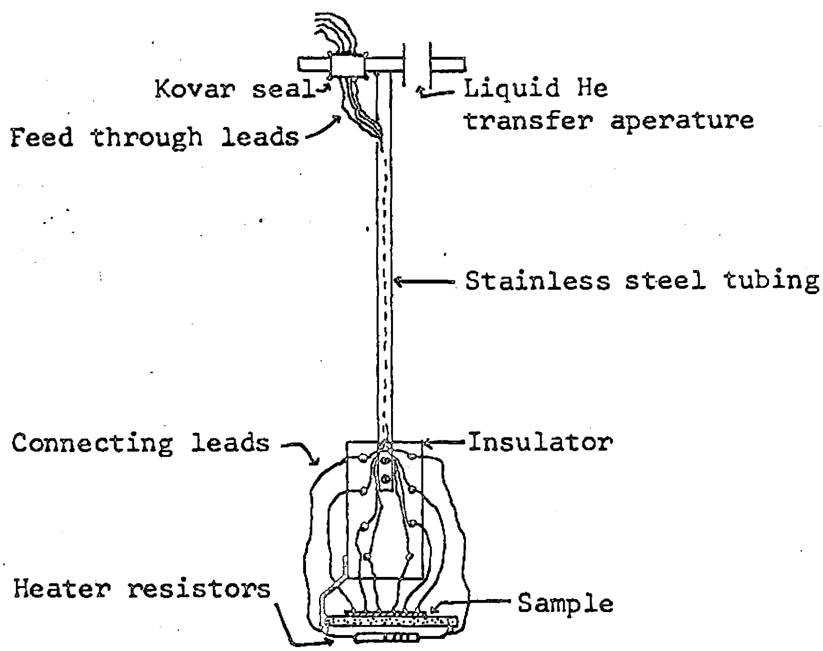

Figure 2.2 Sample holder

helium. The system is arranged in such a way that the helium is recovered after the experiment. The absolute pressure at the surface of the liquid-helium bath is usually measured with a mercury manometer and then transcribed to the corresponding bath temperature with the aid of Bureau of Standards Conversion Tables.

Connected to the cryostat by means of a 3/4" pumping line is a Welch model 1402 duo-seal vacuum-pump with a speed of 140 litres/min. With this pump it is possible to reduce the temperature of the liquid-helium bath to about 2^oK. As the pressure is lowered the temperature of the entire bath is lowered uniformly because convection currents in the liquid helium rapidly bring warm layers to the surface where they boil off.

The over-pressure valve (a rubber tubing with a pinch cock) is a safety device which can be opened if the cryostat pressure significantly exceeds atmospheric pressure. The inlet valve is used to fill the inner dewar of the cryostat with helium exchange gas before liquid helium is transferred into it. Any other gas condenses out when the liquid helium begins to collect in the dewar.

The holder upon which the sample is mounted is shown in Figure 2.2. This consists of thin-walled stainless-steel tubing 1/8" in diameter, the top end of which is soldered to the movable part of the cryostat head, while the bottom end is connected to a piece of non-conducting thin board on which the sample under study is mounted. In the head is mounted a 3/4" Kovar steal with eight electrical feed-through leads and a tube into which the liquid-helium transfer tube can fit. The electrical lead connections from the Kovar seal to the sample are No. 38 insulated copper wires. In addition to the six leads to the sample, there are two more leads which are connected to a heater, consisting of four, half-watt, 47 ohm resistors in parallel, on the under side of the sample holder, to boil off the remaining liquid helium after the experiment. It is also necessary to pump out the helium gas afterwards from the inner dewar, to avoid the danger of helium gas diffusing into the vacuum between the walls of the inner dewar, when the system warms up to room temperature.

2.3 Fabrication of Tunnel Junctions

(A) Choice of Metals:

One of the prime aims of this thesis was an experimental study of the basic physical characteristics of the superconducting tunnel junctions as might be applicable to electric networks. Thus out of the four cases described in Section 1.3(A), the one with two different superconducting metals suggest circuit applications from its characteristic similarity (Figure 1.1(c)) to that of the semiconducting tunnel diode. It should also be noted that the two metals chosen must have widely different energy gaps (i.e. with widely different transition temperatures, since $2\Delta(0) \approx 3.52\ kT_{cr}$, Equation 1.3) for the negative-conductance region to appear prominantly.

In view of the use of the oxide of one of the metals as the tunneling barrier, aluminium would be a ready choice for the first metal, because of the ease in oxidation of aluminium. Nevertheless, T_{cr} of aluminum is $1.2^{o}K$ and the available cryostat could produce temperatures down only to $2^{o}K$. Hence, the choice is limited to those metals which have T_{cr} greater than $2^{o}K$.

At the first sight it may seem convenient to choose metals having critical temperatures higher than the liquid-helium bath temperature, for example, Vanadium ($5.03^{o}K$), Lead ($7.2^{o}K$), Technetium ($8.22^{o}K$, Niobium ($9.09^{o}K$) or many other alloys, such as $NbTc_3$ ($10.5^{o}K$), V_3Si ($17.1^{o}K$), Nb_3Al ($17.5^{o}K$), Nb_3Sn ($18.05^{o}K$)[36]. Giaever[37] reported tunneling into niobium film, showing a large amount of smearing in the characteristic. He mentioned, "This may be interpreted that the film has a filamentary structure, although this is by no means a proof that this is so". Cohen, et al[38] experimenting on chemically deposited tunnel junctions of niobium stannide-lead reported that the junctions were invariably found shorted, including the samples tried with mechanical polishing.

It is well known that a cross-film cryotron (CFC), which employs a tin gate film crossed by a much narrower lead control, can perform both as a digital switching element and as a small-signal amplifier. These CFC's received a wide-spread consideration after the publication of Buck's paper[39] in 1956. A more complete account of subsequent improvements in CFC's is given by Edwards and Newhouse[40]. Basically, the structure of the tunnel junction described earlier is similar to that of CFC except in the former case the insulator is quite thin compared to that in the latter. This similarity suggests that it might be worth while to carry the investigations on tunnel junctions using the same metals, which are used in CFC's.

(B) Oxidation Time and Junction Area:

Once the two metals forming the junction are fixed, say, tin and lead as in the present series of experiments, the "peak point voltage" and the "valley point voltage" are fixed at $(\Delta_2 - \Delta_1)/e$ and $(\Delta_2 + \Delta_1)/e$ respectively, as long as the temperature is kept constant (Section 1.3).

It may be recalled from the semiconductor tunnel diode literature that the greater the peak-to-valley current ratio the greater will be the output current swing[41].

High values of this ratio could be achieved by reducing the insulating oxide thickness and increasing the junction area. However, there is a limit to these two controlling parameters, because of the probable occurrence of shorts from one metal to the other. A number of samples were tried in order to achieve a high value for this ratio, but the characteristics showed up shorts on cooling below the critical temperature of tin. These trials lead us to fix the junction area at about 1 mm^2 and the oxidation time at about 2¼ hours for suitable insulator barriers (see the following section).

(C) Preparation of the Junctions:

A suitable tunnel junction is obtained by vacuum deposition of metal films on a substrate. It is extremely important that the substrate be thoroughly cleaned, since any grease or other organic material may prevent the film from adhering to it. The substrates used in these experiments are flame polished microscope slide sections approximately an inch square. The slide is initially outgassed in a vacuum oven and then cleaned with cleanser and hot water. It is rinsed thoroughly with distilled water and is dried off by wrapping it in lint-free paper tissues. After this the substrate is not touched by hand. The slide and the mask, which determines the geometry of the metal film to be formed, are placed in the slots provided on the substrate mount in the bell-jar.

Tin and lead are usually evaporated from a molybdenum "boat" in a vacuum of 10^{-6} to 10^{-5} torr and deposited on the substrate at a rate of 15 Å/sec. to 200 Å/sec. The lower the pressure, the slower the evaporation rate can be without contaminating the film. It is not necessary to attain a pressure less than 10^{-6} torr, since a trace of gas seems to aid the intermolecular forces which cause the films to adhere to the substrate[40]. Very thin films of some metals (particularly tin) tend to agglomerate on deposition because of surface tension. Since this is a function of the ratio of the substrate temperature to the boiling temperature of the metal, it can be avoided by cooling the substrate sufficiently or by performing the evaporation at a higher temperatures for a shorter time.

The method adopted for oxidation of tin films is to keep the slide after deposition of tin, in an oxidation chamber, through which a stream of oxygen passes freely, at room temperature for a noted time depending upon the thickness required. Alternately, lead may be deposited first and oxidized. Such experiments were reported by Walmsley[34], who used a similar oxidation chamber at higher operational temperature ($\sim 75^{\circ}C$) to oxidize lead. Attempts to fabricate low barrier resistance samples usually resulted in shorts, however, due to the high evaporation temperature required for tin. Nevertheless, such oxidation at higher temperatures is adopted in making lead-lead tunnel junctions, which are used to plot the derivative characteristics (Section 3.2).

After oxidation the slide, together with a proper mask, was mounted back in the evaporator, and the second metal, lead,was deposited to form a cross with the first film.

A total of 52 samples were fabricated during the series of experiments conducted. The following procedure and values were arrived at from trial and error. Typically, two tin strips were deposited first at a pressure of 10^{-5} torr by passing a current of 53-54 amperes at 12V through a molybdenum boat for 15-20 seconds. In this way the milky appearance on the tin film, which shows agglomeration, could be avoided. It was also found that the formation of the required oxide thickness was more effective when the first-evaporated tin film was reduced in thickness to 500 Å - 700 Å. An oxidation time of 2¼ hours was allowed to give a barrier resistance of about 4-5 ohms. For a convenient peak-to-valley current ratio discussed previously, from the circuit application point of view, the barrier resistance should be between 1 and 10 ohms. It was found that better results were obtained if the deposition of the second metal was not delayed too long in waiting for the chamber (evaporator) pressure to become very low, in which case the oxide might grow further. Usually the evaporation of lead was conducted in a pressure of 3 or 4 x 10^{-5} torr. The deposition of this second metal was very critical. If the evaporation current was less than 30 amperes, the time required to form a continuous film was long, resulting in a punch through the oxide layer. The same situation was encountered with higher evaporation current, even though the evaporation time was less. A compromise current of 32 amperes through the evaporation boat for 10-15 seconds gave fairly consistent results.

Reliable electrical contacts to these thin films of lead and tin are made with the aid of a low-melting indium solder without flux. The temperature of a small pencil-type soldering iron is carefully controlled with a variac for this operation. If the iron is too hot, the solder tends to "suck up" the film around it, leaving an isolated solder dot. A cool soldering iron produces cold-solder contacts which "pop-off" when cooled to liquid-helium temperatures. Direct contact between the soldering rion and the film can be avoided by dangling a drop of hot solder from the iron and dragging it over the clean metal until it wets the film.

2.4 DC Voltage Sweep Circuit for I-V Curve Plotting

For plotting the I-V characteristics of the prepared tunnel junctions, a DC voltage sweep circuit is used as shown in Figure 2.3. The potential division of the power supply voltage by a 1 KΩ rheostat, R and the dropping resistor, R_d (1.5Ω, 0.75Ω or 0.3Ω) provide a small, adjustable voltage, in the order of mV. The superconducting tunnel junction is biased by this voltage across R_d. A measuring resistor, R_m, is included in series with the junction. R_m is chosen to be smaller than the junction barrier resistance so that the junction looks into a "constant voltage source". Thus it is possible to trace the complete shape of the I-V characteristic, without any "hysteresis loop" in the negative conductance region.

The power supply voltage can be varied by a built-in control and the circuit parameters are also variable to cope with the insulating barrier resistance of the tunnel junction, which may vary from about

1Ω to 30Ω. DC amplifiers are used, to amplify voltages across R_m and the junction when the barrier resistance exceeds 30Ω. These amplifiers are Dymec type DY-2460A, having a variable gain from 1 to 10^5.

The current through the junction and the potential developed across it are monitored on the Y- and X-axes respectively, of a Moseley type 135C X-Y recorder. Coaxial cables are used for all external connections.

2.5 Harmonic Detection Circuit for dI/dV -V and d^2I/dV^2 -V Plotting

This circuit for measurement of first and second derivatives of I-V plots was originally designed by Dynes and Campbell and is described in detail by Dynes[35]. The same circuit is adopted in the present investigations with the exception of the selective amplifier. The 1 KHz tuned amplifier used for this purpose is designed to achieve a better low-noise performance in plotting the derivative characteristics. The design details of this amplifier are presented in the next section and the present section describes the method and general layout of the circuit adopted.

This method applies a small-amplitude sinusoidal modulation signal, $V_1 \sin \omega t$, to the tunneling junction at a frequency $f = \omega/2\pi$ and detects the resulting current through the junction at f or harmonics of f, by using a narrow-band tuned amplifier and a lock-in amplifier (PAR type). The output of the lock-in is displayed on the Y-axis of the recorder, while the DC bias is plotted along the X-axis. The essentials of the circuit are shown in Figure 2.4. The AC modulation circuit and the DC circuit are connected in parallel. The reference signal to the

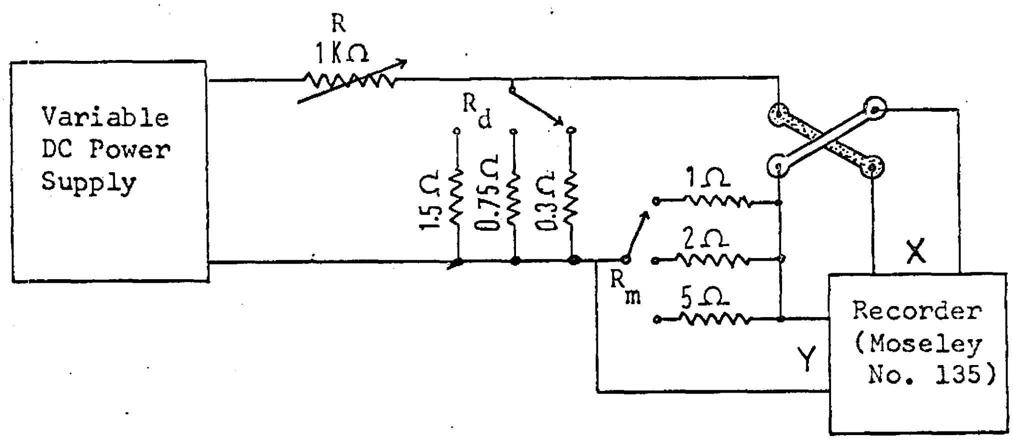

Figure 2.3 DC Circuit for I-V characteristic measurements

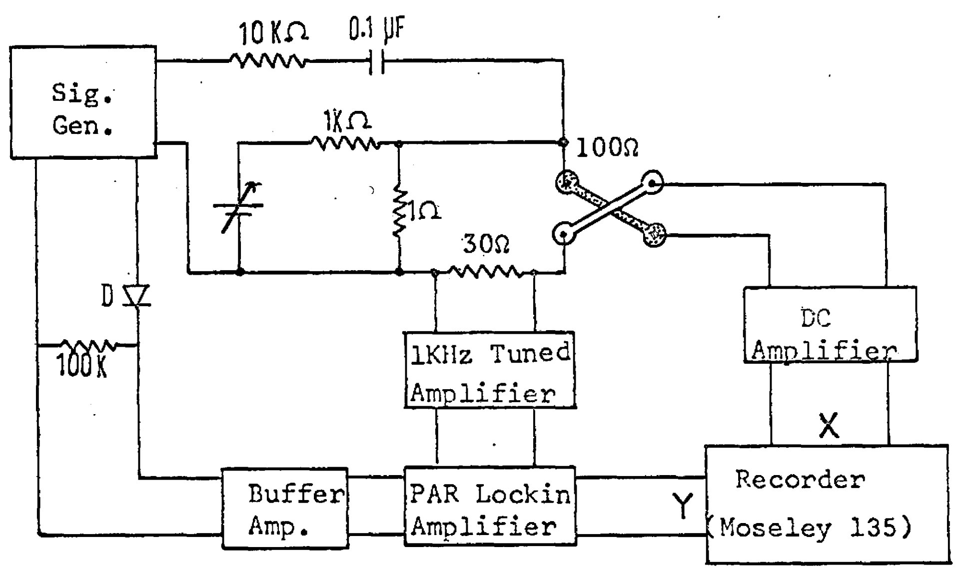

Figure 2.4 Harmonic detection circuit for derivatives measurement.

PAR lock-in amplifier is applied from the same signal generator through a rectifying diode. Typical values of the DC circuit parameters are included to illustrate that the junction now "sees" a low-impedance power source. The barrier resistance of the junction is usually made high for these derivative plots, unlike those junctions fabricated for the circuit application purposes. If the barrier resistance is of the order of 30Ω, the tuned amplifier, whose optimum source impedance is 30Ω (see next section), can be directly connected across the junction itself, because in the range of interest (phonon spectrum) the junction conductance is fairly constant. Coaxial cables are used for all external connections. Further, to minimize pick-up troubles, all the instruments are grounded through a common circuit path to a quiet earth ground and are not connected to the third pin point of the 3-wire 60 cps power outlet.

The theory of harmonic detection is as follows: Let the potential applied across the junction be

$$V = V_o + V_1 \sin \omega t = V_o + \delta V \qquad 2.1$$

where V_o is the DC bias and V_1 is the amplitude of the modulating signal. The current flowing through the junction can be expressed in the form of Taylor's series:

$$I(V) = I_o + \left(\frac{dI}{dV}\right) \delta V + \frac{1}{2!} \left(\frac{d^2I}{dV^2}\right) (\delta V)^2 + \frac{1}{3} \left(\frac{d^3I}{dV^3}\right) (\delta V)^3 + \ldots. \qquad 2.2$$

where I_o is the DC current corresponding to the DC bias V_o. The expression for I(V) can be expanded further:

$$I(V) = I_o + \left(\frac{dI}{dV}\right) V_1 \sin \omega t + \frac{1}{2!} \left(\frac{d^2I}{dV^2}\right) V_1^{\,2} \sin^2 \omega t + \ldots$$

$$= \left[I_o + \frac{1}{4}\left(\frac{d^2I}{dV^2}\right) V_1^{\,2} + \frac{1}{64}\left(\frac{d^4I}{dV^4}\right) V_1^{\,4} + \ldots\right]$$

$$+ \left[\left(\frac{dI}{dV}\right) V_1 + \frac{1}{8}\left(\frac{d^3I}{dV^3}\right) V_1^{\,3} + \ldots\right] \sin \omega t$$

$$+ \left[-\frac{1}{4}\left(\frac{d^2I}{dV^2}\right) V_1^{\,2} - \frac{1}{48}\left(\frac{d^4I}{dV^4}\right) V_1^{\,4} - \ldots\right] \cos 2 t + \ldots \quad 2.3$$

Clearly, the signal at frequency ω will have contributions from higher odd derivatives as well as the first derivative of the I-V characteristic. It can be shown that if the modulating signal is small enough, the most significant contribution at ω is due to the first derivative term, (dI/dV). Similarly, the most significant term at 2ω is the second derivative term, (d^2I/dV^2). In Section 1.3(c), in which the purpose of such derivative characteristics is discussed, it is indicated that the modulation signal should be of the order of kT (86 μV). This justifies the above assumption of a small enough signal.

2.6 Design and Construction Details of 1 KHz Tuned Amplifier

(A) Purpose and Description:

The amplifier designed and constructed during this project is a sensitive, low-noise amplifier tuned to 1 KHz. This is intended to select the 1 KHz voltage component out of a superconducting tunnel junction (if the barrier resistance is of the order of 30Ω) or a measuring resistance, when a very low-level modulating signal (f = 1 KHz or 500 Hz) is superimposed on the DC bias. This component is proportional to the first or second derivative of the tunnel current depending upon whether the selection is made at f or 2f (see the previous section).

The amplifier consists of four parts, viz, a low-noise input stage, a differential amplifier, an emitter-follower output stage and a twin-T notch filter in the feedback loop to achieve the selectivity at the desired frequency of 1 KHz. The amplifier is fed through an input transformer to provide better impedance matching with low-impedance sources. The overall gain of the amplifier (together with the transformer) is 70 dB and the sensitivity of the system at the tuned frequency is 65 nV for a 10 dB S/N ratio at the output. The complete schematic circuit diagram is shown in Figure 2.5.

(B) Design Approach:

(i) INPUT STAGE

The overall noise performance of an amplifying system is mostly governed by its input stage. An NPN diffused silicon planar, low-level, low-noise type 2N2484 transistor is chosen for this purpose. From the data sheets of this transistor (Fairchild), it can be seen that if the transistor is operated at a collector current of less than 20 μA, the corner frequency of the 1/f noise is about 100 Hz. Thus, at the operating frequency of 1 KHz the transistor exhibits only shot noise. Further if the transistor is operated at a collector current of about 2 μA, the noise figure is minimum at a source resistance of about 50 KΩ (NF is

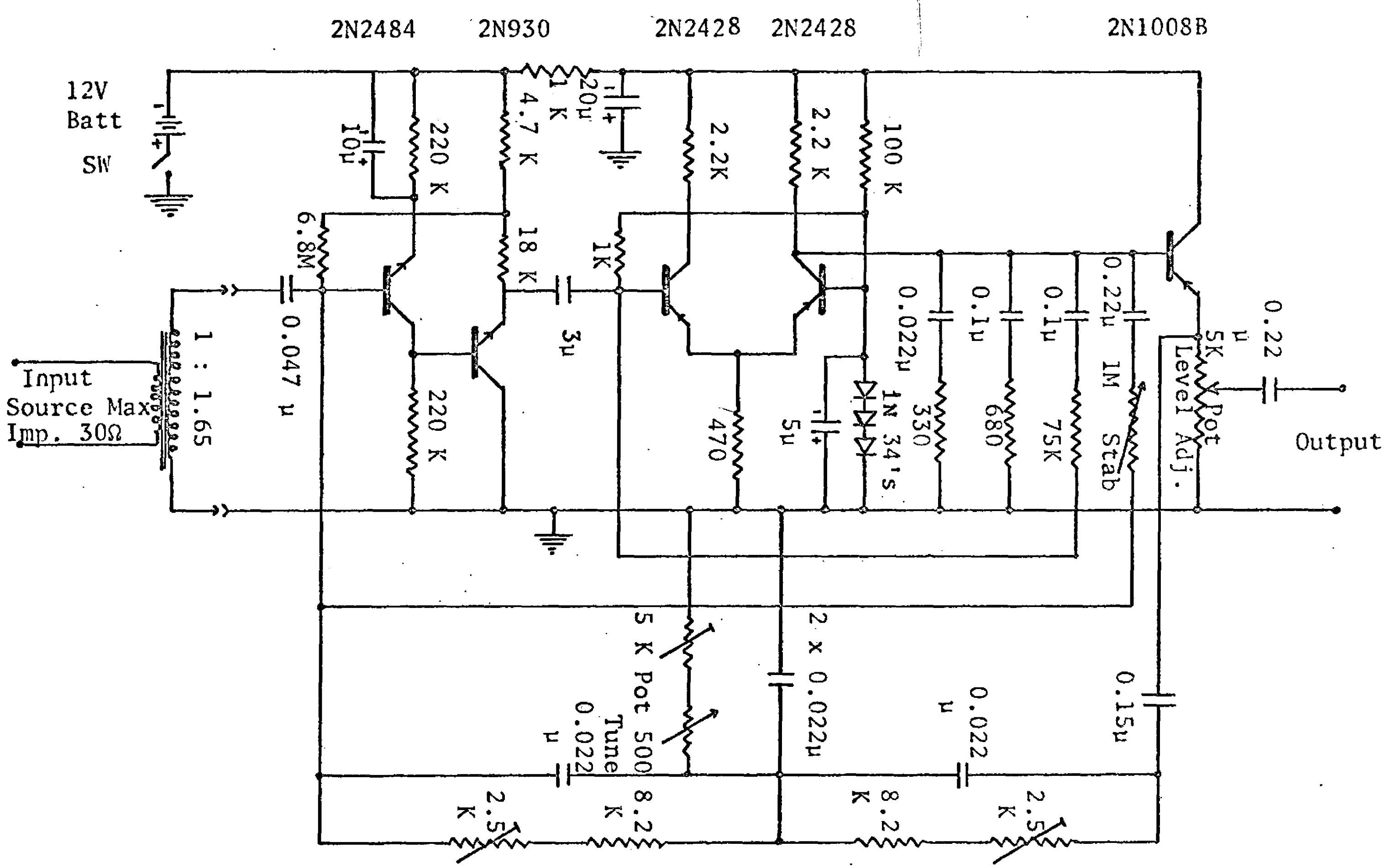

All resistors in ohms and all capacitors in farads

FIGURE 2.5: Schematic Circuit Diagram of 1 KHz Amplifier

nearly constant from 40 to 60K). With these specifications and with a frequency of operation at 1 KHz, the noise figure of the transistor lies within the 1 dB contour of narrow-band noise figure. The current amplification factor h_{fe} of this transistor is about 200 even at this low I_c.

The high source impedance is provided by a Keithley model 1034 well-shielded input transformer with a 1.65 turns ratio. A 133 K Ω resistor is soldered across the secondary of the transformer (inside the shielded box) and thus the recommended maximum source resistance is 30 ohms. Therefore, the dynamic resistance of the tunnel junction or the series measuring resistor, across which the low-level signal is detected, could be varied from 20 to 30 ohms, while still retaining the low-noise figure of the input stage.

Since the amplifier is now looking into a high-impedance source, in order not to load the input signal, the input impedance of the first stage is raised to about 150 KΩ by the use of negative feed back applied to a common-emitter-common-collector cascade. Another low-noise NPN planar type 2N930 transistor (T_2) is closely coupled with a 2N2484 transistor (T_1) as a bootstrap arrangement to form the cascade with the required feed back. Compared to this close coupling of T_2, the effect of other feed back networks (twin-T and the RC's for phase margin adjustment --described later) is small, because these are across the total amplifier.

A passing remark about the choice of the input stage may be made. A 2N3069 N-channel field-effect transistor was tried for the input stage in a configuration such as described by Munoz[42] and where the high source impedance was provided by the available Keithley 1034 transformer. The noise performance was found comparable with that of the 2N2484 operated at the above mentioned low collector current. It may be noted that the 2N3069 FET has a noise figure no better than 2 dB and that the 1034 transformer cannot provide the high source impedance required by this FET. Thus from these observations it may be concluded that if a FET such as 2N3460 and a transformer with a higher turns ratio are chosen, a better noise performance might be obtained.

(ii) DIFFERENTIAL AMPLIFIER AND EMITTER FOLLOWER

The second stage of the amplifier is a differential or balanced amplifier. This amplifier provides direct coupling and low drift. The emitters of the two transistors, T_3 and T_4 (type 2N2428, PNP) are coupled through a common resistor, which forms a constant-current tail. A low drain bias for the bases of T_3 and T_4 is formed by a 100 KΩ resistor and three series connected germanium diodes (type 1N34). This method provides a fairly constant bias with a minimum load on the supply battery. The biasing diodes are bypassed by a 5 μf capacitor, so that the T_4 base forms the reference point and the signal is fed to the T_3 base from the T_1-T_2 feedback pair. The transistor T_5 (type 2N1008B, PNP) is connected as an emitter follower so that the output signal of the amplifier can be obtained across a low impedance and can conveniently be coupled to the input of the next lock-in amplifier unit. The potentiometer in the emitter lead facilitates the output level variation without altering the impedance level of any of the stages.

(iii) TWIN-T NOTCH FILTER

The feedback loop of the amplifier is a twin-T rejection network.

This notch filter feeds back all other frequency components of the signal at the output of the amplifier, with a phase reversal to the input, except that at the notch frequency to which the filter is tuned. Thus the amplifier becomes selective at this tuned frequency.

Although other combinations of components may be used, the one shown in Figure 2.6 has the greatest possible selectivity. With this general configuration, any filter exhibits infinite attenuation at the notch frequency f_o, which is satisfied by the values of R anc C. If the aim is only to reject f_o, then the choice of these values is arbitrary. If a symmetrical response is sought after on the other hand, the choice of components may be established easily with the aid of two recently published nomographs[43] based on the equations 2.4 and 2.5

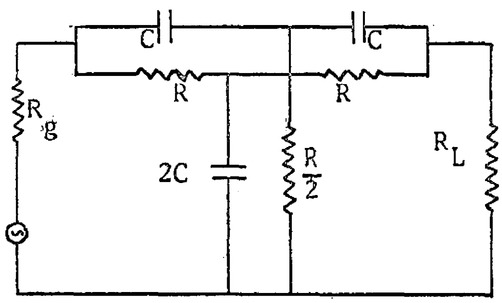

$$R = (2 R_g R_L)^{\frac{1}{2}} \qquad 2.4$$

$$f_o = \frac{1}{2\pi RC} \qquad 2.5$$

FIGURE 2.6: Twin-T Notch Filter

The input and output impedances are determined approximately by the "loading" method and are found to be 800Ω and 60 KΩ, respectively, (with the input transformer connected). If the notch frequency is chosen to be 1 KHz, then from the nomographs, the values of R and C are found to be about 8 KΩ and 0.022 μf respectively. Low-value variable potentiometers are provided in all resistor-arms for minor adjustments. The one in series with the shunt resistor is returned to the front panel for "tune" adjustment.

(iv) PHASE-MARGIN

Since the amplifier gain is large enough, when the twin-T feedback loop is connected, the system may become unstable and thus give rise to oscillations, at roughly the twin-T notch frequency. Thus it becomes necessary to adjust the loop phase-margin of the amplifier, so that the complete system is stable[44].

The adjustment of the phase-margin is achieved by a two loop feedback arrangment with CR networks as shown in the schematic of Figure 2.5. One of the resistors of these feedback loops is returned to the front panel of the instrument for final "stability" adjustment. The adjustment of this resistance and the twin-T components is rather involved in the sense that as the stability resistor is varied, the impedance levels of the amplifier change slightly, and thus the twin-T has to be altered accordingly for sharp tuning.

After final adjustments, the stabilizing and tuning controls are locked. In the course of operation, therefore, it may be necessary to align the signal frequency for optimal tuning.

(C) <u>Measurements:</u>

The selective response of the amplifier is shown in Figure 2.7. The over all gain of the amplifier at the tuned frequency is 70 dB, which includes the step-up-ratio of the input transformer (about 20 dB when loaded with the input of the amplifier). The first transistor 2N2484, when operated at low-collector current (2μA) contributes to a voltage gain of 20 dB; while the differential amplifier gives a gain of 30 dB.

The 3 dB bandwidth of the amplifier, as can be seen from

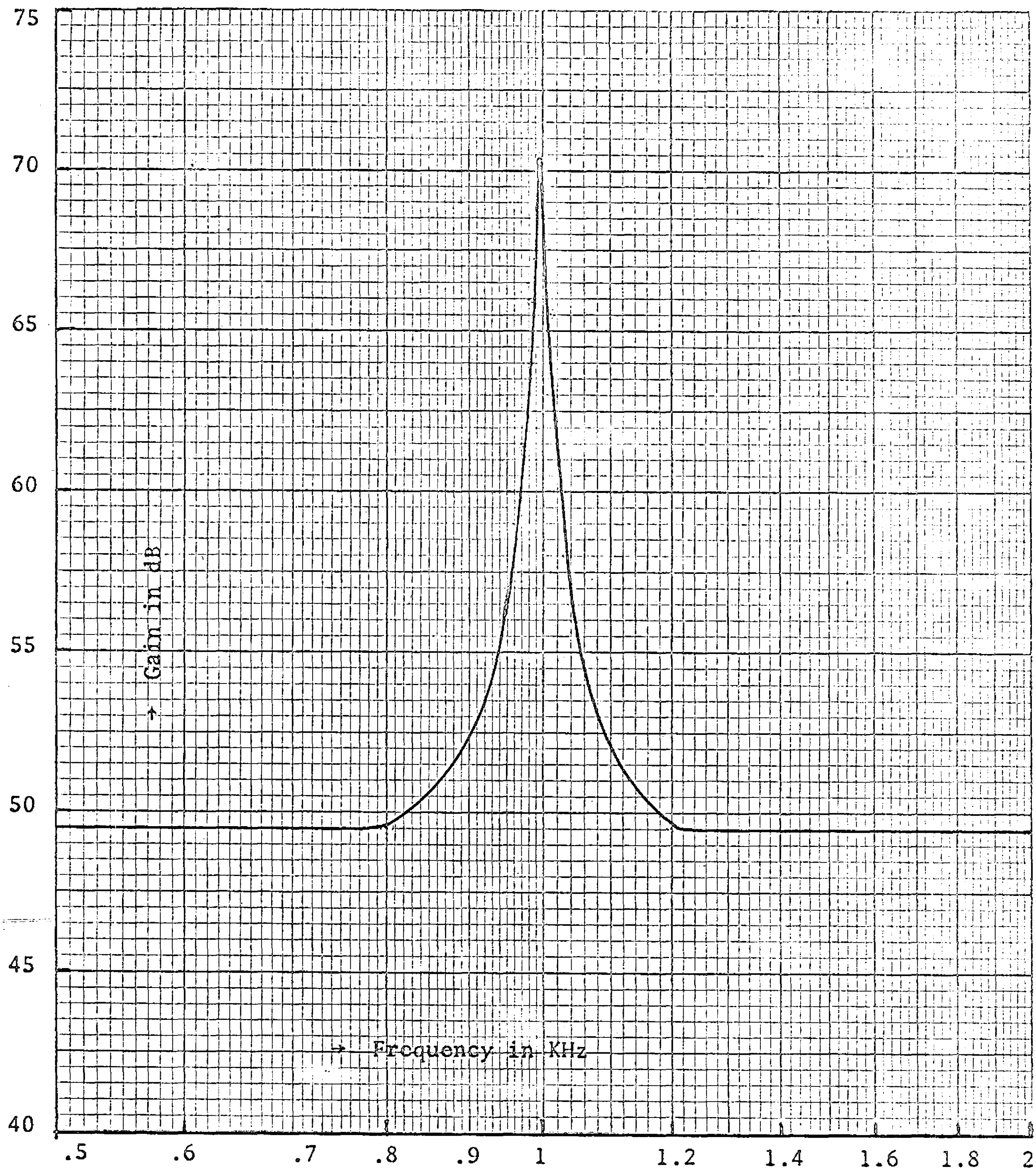

FIGURE 2.7: Frequency Response of the 1 KHz Amplifier

Figure 2.7 is about 8 Hz. The presence of the CR feedback loops effectively increase the bandwidth. However, this could be made narrower by slight manipulation of twin-T components, but this value is retained in view of the stability of the system.

The noise-figure measurement of this amplifier is rather difficult because of the input transformer and the twin-T feedback network. Thus the noise character of this amplifier is expressed in two convenient ways.

(i) The noise level of the amplifier is about 1×10^{-8} volts referred to the input of the transformer, when it is shunted with a 30 Ω resistance (which is the recommended maximum source resistance).

(ii) The sensitivity of the amplifying system is 6.5×10^{-8} volts at the input fed from a 30 Ω source, for a 10 dB S/N ratio at the output of the amplifier.

CHAPTER 3

STATIC AND DERIVATIVE CHARACTERISTICS OF SPECIFIC TUNNEL JUNCTIONS

3.1 Static Characteristics

(a) I-V Characteristics:

The tunnel junctions studies in this project consisted of tin-tin oxide-lead sandwiches. Tin has a transition temperature of $3.72^{\circ}K$, while that of lead is $7.2^{\circ}K$. Thus the lead film becomes superconducting as soon as the sample is introduced in a liquid-helium bath. This can be seen from the I-V curve for $4.24^{\circ}K$ operation as shown in Figure 3.1(a). As the liquid-helium bath temperature is reduced, the I-V characteristic changes gradually to show up the negative-resistance region, which is effected when the tin film becomes superconducting. As the temperature is further reduced the energy gap of tin increases, resulting in a wider negative-resistance region. This is very well illustrated in Figures 3.1(a) and (b).

(b) Energy gaps from I-V Characteristics:

Referring to Figure 1.1 and to the discussion on the density-of-states function, we recall that N-S samples do not readily give exact information on the energy gap, but S-S samples should give a well-defined cusp in the characteristic at $(\Delta_2 - \Delta_1)/e$ and a sharp rise at $(\Delta_2+\Delta_1)/e$. The results for $2\Delta_{Sn}$ obtained from Figure 3.1 and similar figures on other samples are presented in Figure 3.2. The solid line is a BCS plot of the energy gap as a function of temperature, fitted to the values: $T_{cr} = 3.72^{o}K$; $2\Delta_{Sn}(0) = 1.02$ meV. The compatability of the results is quite good.

(c) Comparison of Theoretical and Experimental I-V Curves:

The theoretical values (as based on the analysis presented in Section 1.3(B)) for tunneling current at different bias points for the case of a tin-lead junction with lead only superconducting ($4.24^{o}K$), are calculated using a Gauss-Laguerre (GLIN 14) type numerical integration on IBM 7040 computer. Similar calculations are performed for the case of both tin and lead superconducting at $3.65^{o}K$, using a Gauss (GINT 14) type integration. The values used for energy gaps are measured on experimental plots such as given in Figure 3.1. Tables 1 and 2 give the computational results, while Figures 3.3 and 3.4 give a quantitative comparison between the analysis and experiment for Sn-SnO_x-Pb junctions at $4.24^{o}K$ and $3.65^{o}K$ respectively. The experimental points are derived from plots such as in Figure 3.1 and the current values are normalized to fit the curve at the point shown by the arrows. The agreement between the calculated curves and experimental points is extremely good except that the current jump in the $3.65^{o}K$ case is spread over a small region of voltage and that the negative-conductance region is more pronounced in the theoretical curve, because the leakage effects through the practical oxide layer are not included.

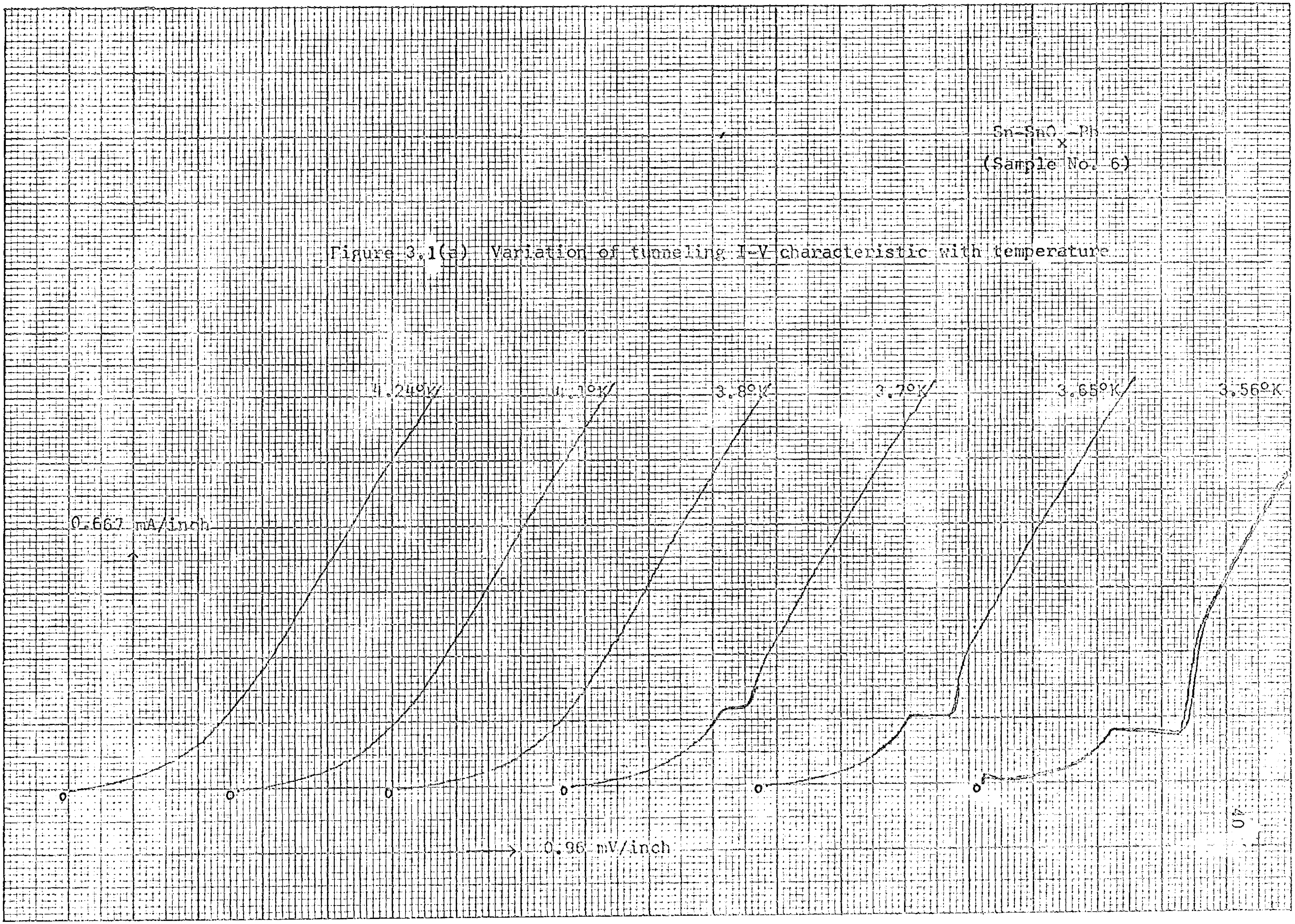

Figure 3.1(a) Variation of tunneling I-V characteristic with temperature

Figure 3.1(b) Continuation of 3.1(a)

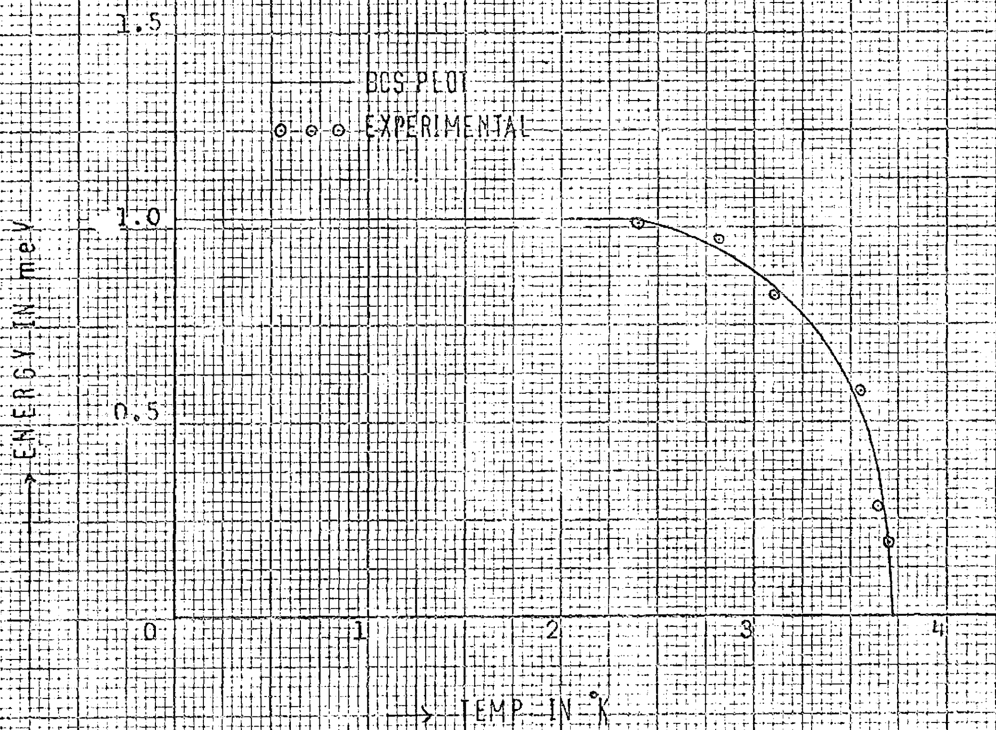

Figure 3.2 Temperature variation of energy gap of Sn

CALCULATIØN ØF TUNNEL CURRENTS IN TIN-LEAD JUNCTIØN AT 4.24

DC BIAS	I1	I2	TUNNEL CURRENT
0.100E-03	0.19694E-01	0.15119E-01	0.34813E-01
0.200E-03	0.45279E-01	0.26701E-01	0.71979E-01
0.300E-03	0.78398E-01	0.35558E-01	0.11396E 00
0.400E-03	0.12108E 00	0.42325E-01	0.16340E 00
0.500E-03	0.17576E 00	0.47488E-01	0.22325E 00
0.600E-03	0.24532E 00	0.51425E-01	0.29674E 00
0.700E-03	0.33299E 00	0.54426E-01	0.38742E 00
0.800E-03	0.44229E 00	0.56713E-01	0.49900E 00
0.900E-03	0.57671E 00	0.58454E-01	0.63517E 00
0.100E-02	0.73945E 00	0.59779E-01	0.79923E 00
0.110E-02	0.93292E 00	0.60789E-01	0.99370E 00
0.120E-02	0.11583E 01	0.61557E-01	0.12198E 01
0.130E-02	0.14151E 01	0.62141E-01	0.14773E 01
0.140E-02	0.17013E 01	0.62586E-01	0.17639E 01
0.150E-02	0.20131E 01	0.62925E-01	0.20761E 01
0.160E-02	0.23456E 01	0.63182E-01	0.24088E 01
0.170E-02	0.26934E 01	0.63378E-01	0.27568E 01
0.180E-02	0.30512E 01	0.63527E-01	0.31147E 01
0.190E-02	0.34140E 01	0.63641E-01	0.34777E 01
0.200E-02	0.37781E 01	0.63727E-01	0.38418E 01
0.210E-02	0.41406E 01	0.63793E-01	0.42043E 01
0.220E-02	0.44994E 01	0.63843E-01	0.45632E 01
0.230E-02	0.48534E 01	0.63881E-01	0.49173E 01
0.240E-02	0.52020E 01	0.63910E-01	0.52659E 01
0.250E-02	0.55446E 01	0.63932E-01	0.56085E 01
0.260E-02	0.58812E 01	0.63948E-01	0.59452E 01
0.270E-02	0.62120E 01	0.63961E-01	0.62760E 01
0.280E-02	0.65376E 01	0.63971E-01	0.66016E 01
0.290E-02	0.68589E 01	0.63978E-01	0.69228E 01
0.300E-02	0.71768E 01	0.63984E-01	0.72408E 01
0.310E-02	0.74920E 01	0.63988E-01	0.75560E 01
0.320E-02	0.78044E 01	0.63991E-01	0.78684E 01
0.330E-02	0.81137E 01	0.63994E-01	0.81776E 01
0.340E-02	0.84188E 01	0.63996E-01	0.84828E 01
0.350E-02	0.87195E 01	0.63997E-01	0.87835E 01
0.360E-02	0.90162E 01	0.63998E-01	0.90802E 01
0.370E-02	0.93101E 01	0.63999E-01	0.93741E 01
0.380E-02	0.96033E 01	0.64000E-01	0.96673E 01
0.390E-02	0.98978E 01	0.64000E-01	0.99618E 01
0.400E-02	0.10195E 02	0.64000E-01	0.10259E 02
0.410E-02	0.10493E 02	0.64001E-01	0.10557E 02
0.420E-02	0.10793E 02	0.64001E-01	0.10857E 02
0.430E-02	0.11090E 02	0.64001E-01	0.11154E 02
0.440E-02	0.11382E 02	0.64001E-01	0.11446E 02
0.450E-02	0.11668E 02	0.64001E-01	0.11732E 02
0.460E-02	0.11948E 02	0.64001E-01	0.12012E 02
0.470E-02	0.12222E 02	0.64001E-01	0.12286E 02
0.480E-02	0.12495E 02	0.64001E-01	0.12559E 02
0.490E-02	0.12770E 02	0.64001E-01	0.12834E 02
0.500E-02	0.13051E 02	0.64001E-01	0.13115E 02

014 V SINHA 020 001MIN 38SEC CØST$007.38 REN. TIME 0015MIN 21SEC

TABLE 1

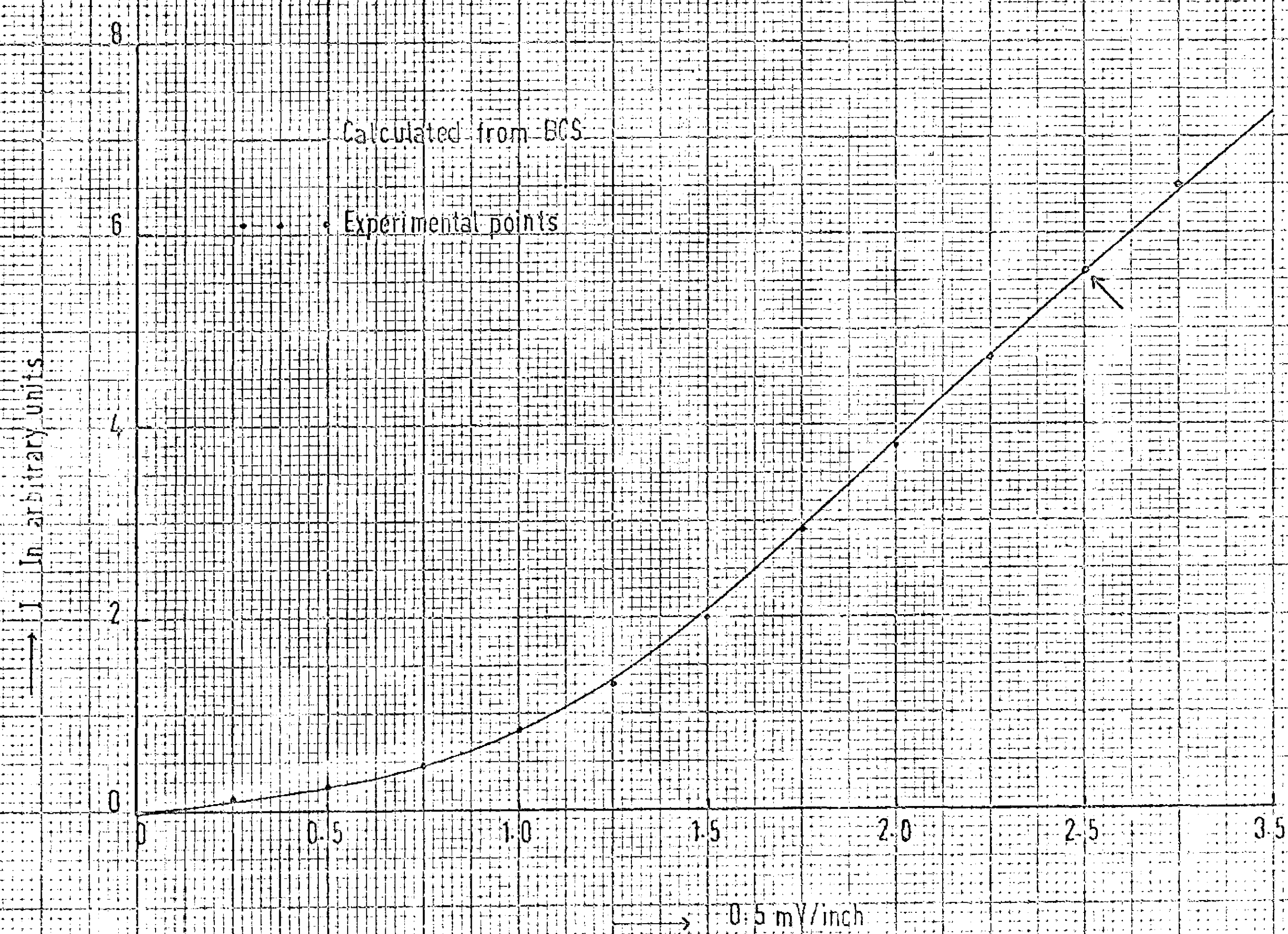

Figure 3.3 Comparison of Tunnel Currents (Tin-Lead Junction at 4.24°K)

TABLE 2

TUNNEL CURRENTS WHEN TIN AND LEAD ARE SUPERCØNDUCTING 2G1=0.286MV,2G2=2.46MV AT 3.65K

DC BIAS	I1	I2	I3	I4	TUNNEL CURRENT
0.100E-03	0.19895E-01	0.14550E-01	0.	0.	0.34445E-01
0.200E-03	0.46964E-01	0.25213E-01	0.	0.	0.72177E-01
0.300E-03	0.83660E-01	0.33008E-01	0.	0.	0.11667E 00
0.400E-03	0.13317E 00	0.38698E-01	0.	0.	0.17187E 00
0.500E-03	0.19958E 00	0.42846E-01	0.	0.	0.24242E 00
0.600E-03	0.28801E 00	0.45867E-01	0.	0.	0.33388E 00
0.700E-03	0.40493E 00	0.48065E-01	0.	0.	0.45300E 00
0.800E-03	0.55881E 00	0.49665E-01	0.	0.	0.60847E 00
0.900E-03	0.76340E 00	0.50827E-01	0.	0.	0.81422E 00
0.100E-02	0.10601E 01	0.51672E-01	0.	0.	0.11118E 01
0.110E-02	0.	0.52286E-01	0.15518E 01	0.	0.16041E 01
0.120E-02	0.	0.52731E-01	0.10728E 01	0.	0.11256E 01
0.130E-02	0.	0.53054E-01	0.94768E 00	0.	0.10007E 01
0.140E-02	0.	0.53289E-01	0.88032E 00	0.13673E 01	0.23009E 01
0.150E-02	0.	0.53458E-01	0.83661E 00	0.18169E 01	0.27070E 01
0.160E-02	0.	0.53581E-01	0.80545E 00	0.22691E 01	0.31281E 01
0.170E-02	0.	0.53669E-01	0.78190E 00	0.27210E 01	0.35566E 01
0.180E-02	0.	0.53733E-01	0.76341E 00	0.31691E 01	0.39862E 01
0.190E-02	0.	0.53778E-01	0.74848E 00	0.36102E 01	0.44125E 01
0.200E-02	0.	0.53811E-01	0.73617E 00	0.40426E 01	0.48326E 01
0.210E-02	0.	0.53834E-01	0.72584E 00	0.44654E 01	0.52451E 01
0.220E-02	0.	0.53851E-01	0.71707E 00	0.48785E 01	0.56494E 01
0.230E-02	0.	0.53862E-01	0.70951E 00	0.52822E 01	0.60455E 01
0.240E-02	0.	0.53870E-01	0.70295E 00	0.56772E 01	0.64340E 01
0.250E-02	0.	0.53875E-01	0.69721E 00	0.60644E 01	0.68155E 01
0.260E-02	0.	0.53879E-01	0.69215E 00	0.64446E 01	0.71906E 01
0.270E-02	0.	0.53881E-01	0.68768E 00	0.68185E 01	0.75601E 01
0.280E-02	0.	0.53882E-01	0.68371E 00	0.71871E 01	0.79247E 01
0.290E-02	0.	0.53883E-01	0.68017E 00	0.75508E 01	0.82849E 01
0.300E-02	0.	0.53883E-01	0.67700E 00	0.79104E 01	0.86413E 01
0.310E-02	0.	0.53883E-01	0.67415E 00	0.82663E 01	0.89944E 01
0.320E-02	0.	0.53882E-01	0.67158E 00	0.86191E 01	0.93445E 01
0.330E-02	0.	0.53882E-01	0.66924E 00	0.89690E 01	0.96921E 01
0.340E-02	0.	0.53881E-01	0.66711E 00	0.93164E 01	0.10037E 02
0.350E-02	0.	0.53881E-01	0.66516E 00	0.96616E 01	0.10381E 02
0.360E-02	0.	0.53880E-01	0.66336E 00	0.10005E 02	0.10722E 02
0.370E-02	0.	0.53879E-01	0.66170E 00	0.10346E 02	0.11062E 02
0.380E-02	0.	0.53879E-01	0.66015E 00	0.10686E 02	0.11400E 02
0.390E-02	0.	0.53878E-01	0.65870E 00	0.11025E 02	0.11737E 02
0.400E-02	0.	0.53877E-01	0.65735E 00	0.11362E 02	0.12073E 02
0.410E-02	0.	0.53877E-01	0.65608E 00	0.11698E 02	0.12408E 02
0.420E-02	0.	0.53876E-01	0.65488E 00	0.12033E 02	0.12742E 02
0.430E-02	0.	0.53875E-01	0.65376E 00	0.12367E 02	0.13075E 02
0.440E-02	0.	0.53875E-01	0.65270E 00	0.12700E 02	0.13407E 02
0.450E-02	0.	0.53874E-01	0.65170E 00	0.13033E 02	0.13738E 02
0.460E-02	0.	0.53874E-01	0.65075E 00	0.13364E 02	0.14069E 02
0.470E-02	0.	0.53873E-01	0.64987E 00	0.13695E 02	0.14399E 02
0.480E-02	0.	0.53873E-01	0.64904E 00	0.14026E 02	0.14728E 02
0.490E-02	0.	0.53873E-01	0.64826E 00	0.14355E 02	0.15057E 02
0.500E-02	0.	0.53872E-01	0.64753E 00	0.14685E 02	0.15386E 02

6014 V SIMHA 020 001MIN 52SEC CØST$008.39 REM. TIME 0013MIN 30SEC

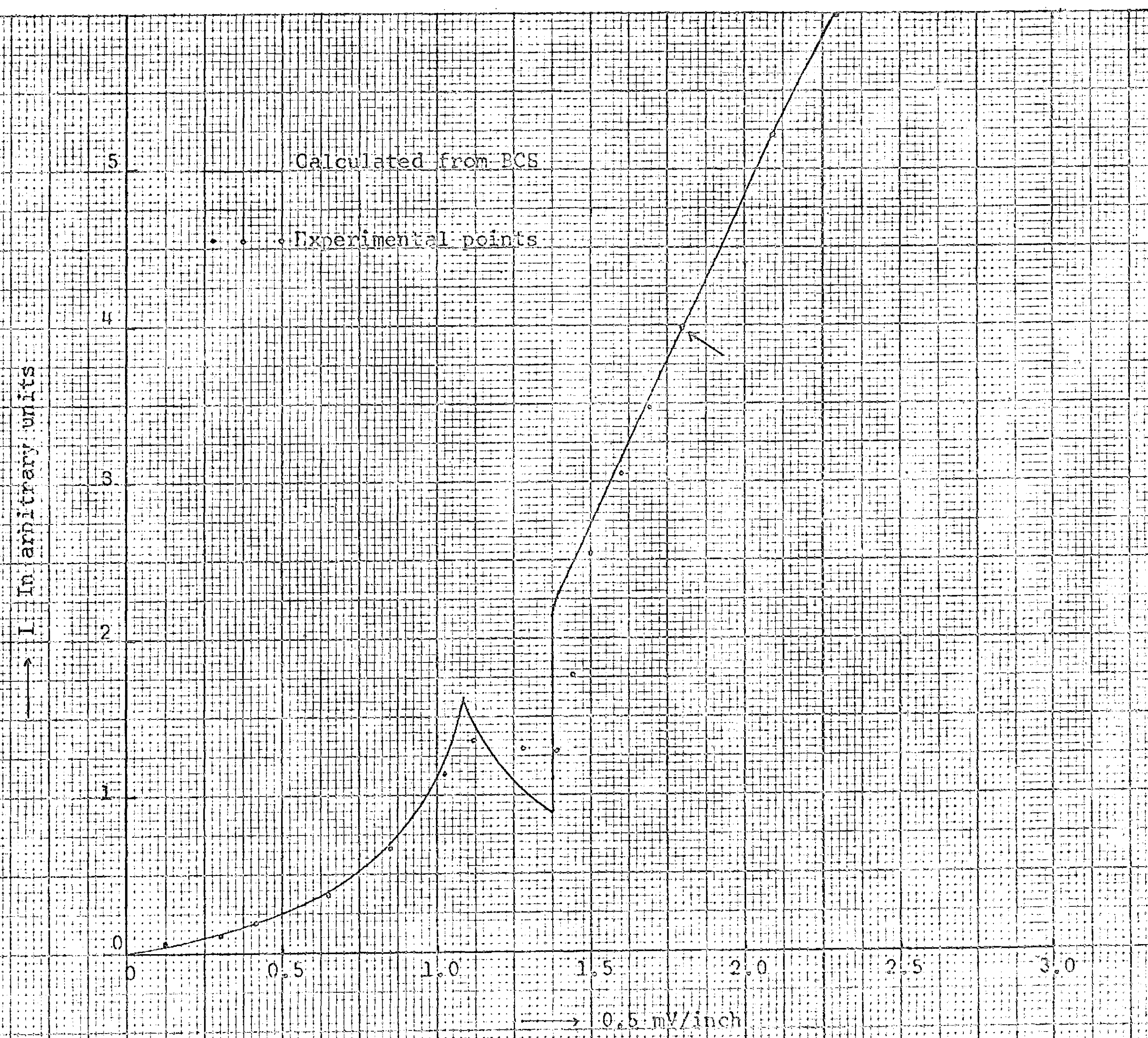

Figure 3.4 Comparison of Tunnel Currents
(Sn-I-Pb at 3.65°K)

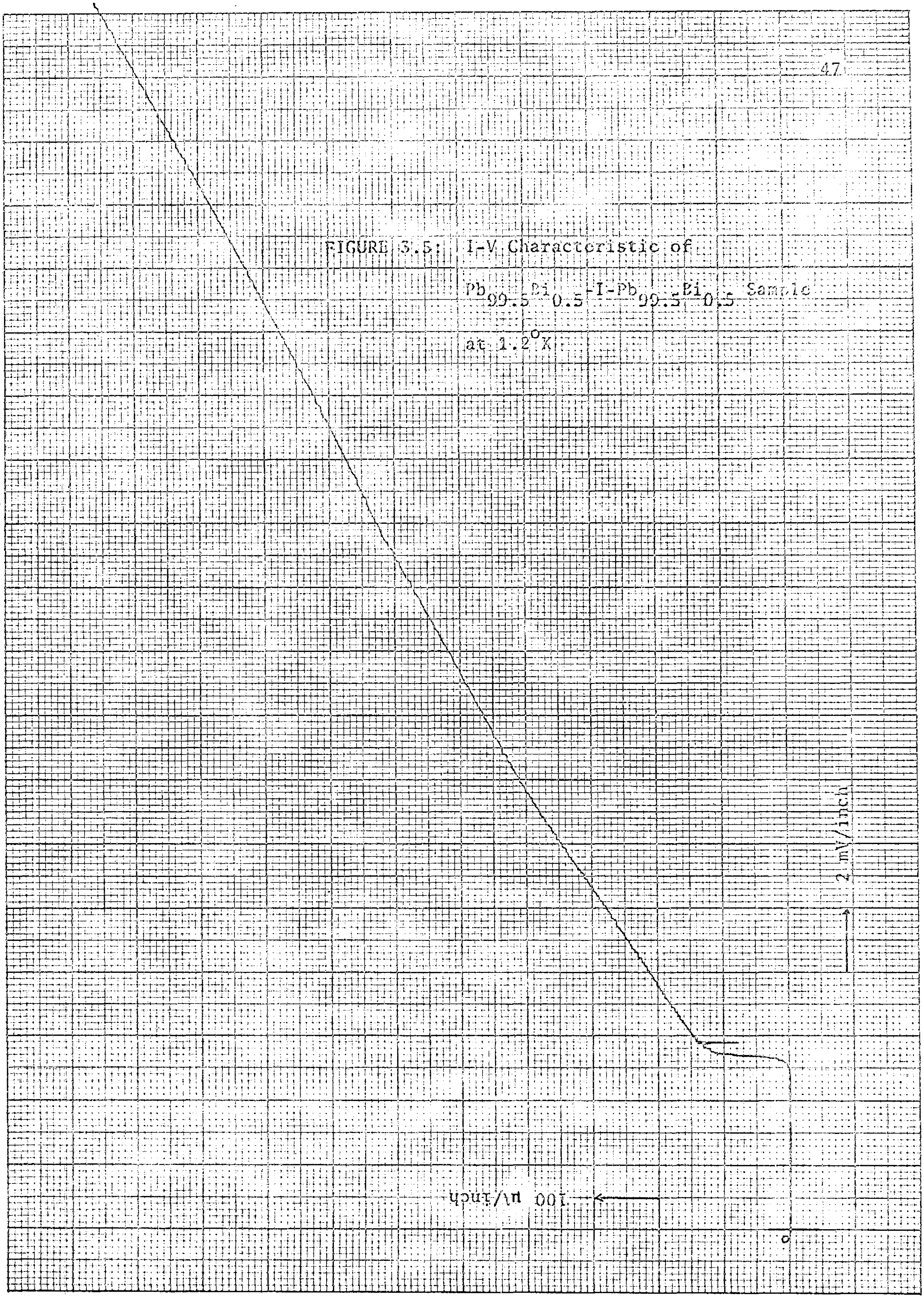

FIGURE 3.5: I-V Characteristic of $Pb_{99.5}Bi_{0.5}$-I-$Pb_{99.5}Bi_{0.5}$ Sample at 1.2°K

FIGURE 3.6: First Derivative Plot of the Curve in Figure 3.5

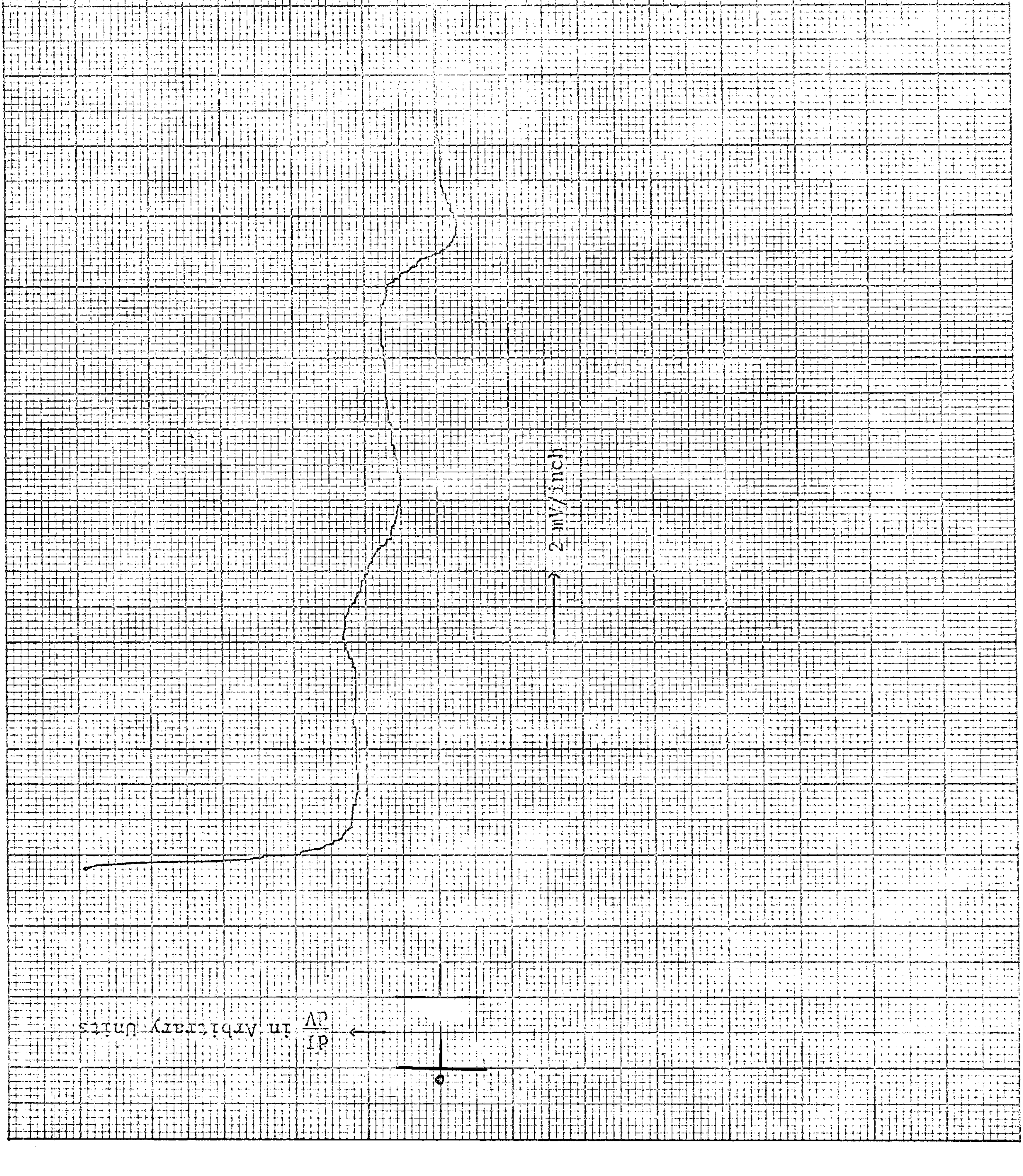

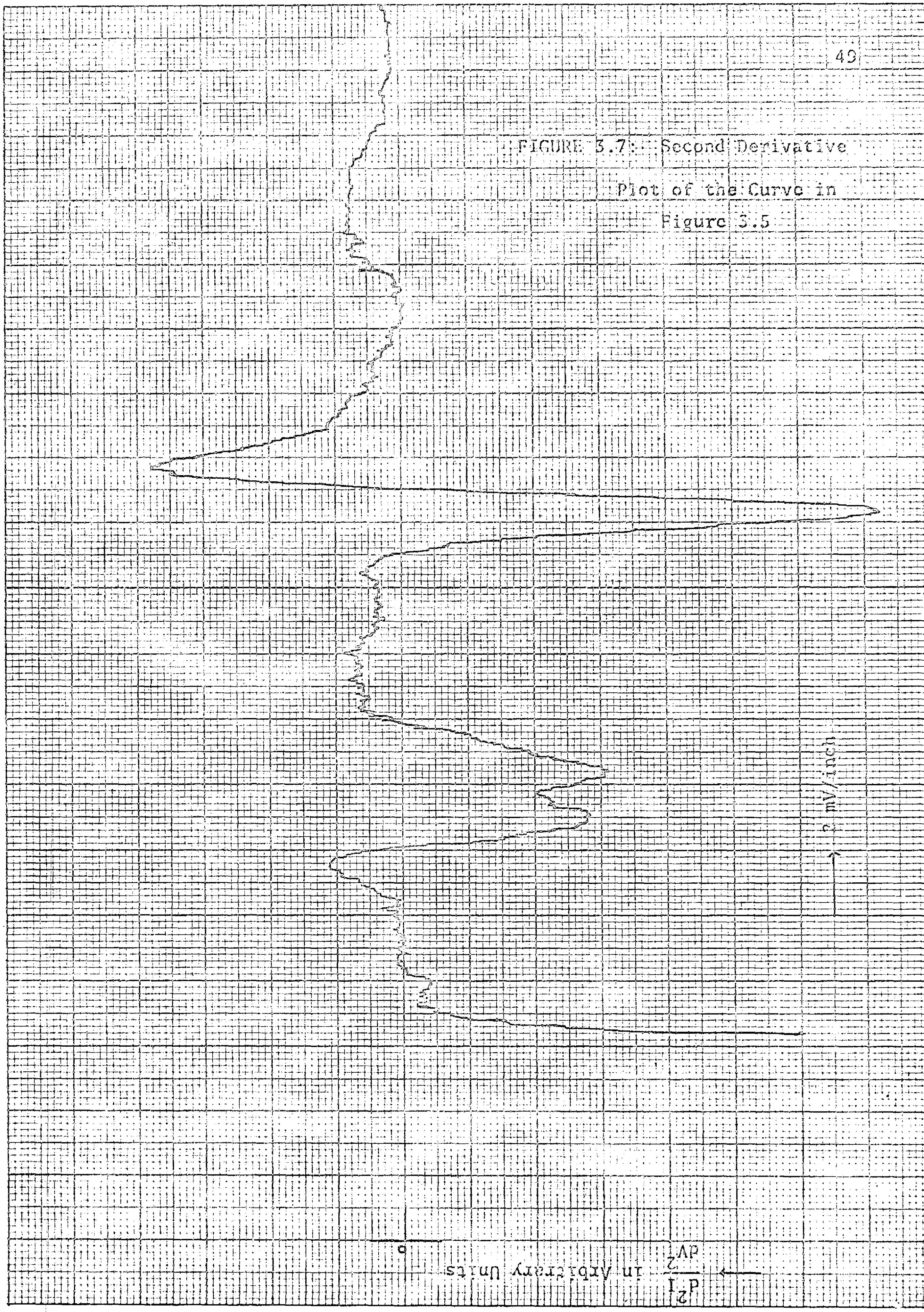

FIGURE 3.7: Second Derivative Plot of the Curve in Figure 3.5

3.2 Derivative Characteristics

The purpose and utility of obtaining the derivative plots of the I-V characteristics have been enumerated in Section 1.3(c) and the electronic circuitry adopted has been described in Sections 2.5 and 2.6.

As pointed out in Section 2.3, it is desirable to fabricate a junction with two identical metals for a detailed study of the derivative characteristics. Thus $Pb_{99.5}Bi_{0.5}$-I-$Pb_{99.5}Bi_{0.5}$ samples were fabricated with each lead alloy film of about 1000 Å and the insulating oxide of about 50 Å. Figures 3.6 and 3.7 are the first (dI/dV) and second (d^2I/dV^2) derivative plots respectively of the I-V characteristic shown in Figure 3.5.

As pointed out in Section 1.3(c) the first derivative plot gives us the effective density-of-states in the tunneling mechanism. From the second derivative plot it can be seen that the transverse and longitudinal peaks occur at 4.4 meV and 8.4 meV, respectively (measured from the energy-gap edge). It may also be noted that the fine structure near the transverse peak and at higher bias is resolved with the low-modulation signal about 50 μV (signal applied was 200 μV, barrier resistances was about 10 Ω and the measuring resistor was 33 Ω-- see Figure 2.4).

CHAPTER 4

POSSIBLE CIRCUIT APPLICATIONS

4.1 Introduction

The use of a two-terminal negative resistance network, synthesized by means of a positive feedback vacuum-tube circuit, for the purpose of amplification was first discussed by Crisson[45] in 1931. The subsequent semiconductor devices such as PNPN transistor, unijunction transistor, four-layer diode and the recent parametric devices were found to exhibit negative resistance. Esaki[46] (tunnel) diode was a startling addition to this family in 1958.

Another device presenting a negative-resistance region in its static characteristic is the double-superconducting-metal junction. The similarity of the characteristic of this kind of tunnel diode with that of the Esaki diode immediately suggests that such a device may be used as an amplifier, an oscillator or a switch. Further, the principle of quantum mechanical tunneling involved in both semiconducting and superconducting tunnel diodes prompts that a comparison of performance of these two devices may be made.

The tunnel diode (semiconducting or superconducting) is a significant and interesting device largely because of its peculiar voltage-current non-linear relationship. The general shape of such a characteristic is shown in Figure 4.1. This curve is appropriately called "voltage-controlled" or sometimes "N-type" or "short-circuit stable". The reason for this latter term can be seen from the load lines for high- and low-impedance biasing circuits. The points of intersection of the characteristic and the load lines represent the possible values of voltage and current consistent with the characteristic in a static DC sense. It may be noted that there are three possible equilibrium points for a high-impedance source, but only one possible point with a low-impedance source. Out of the three points in the former case, the centre one is commonly unstable. Thus the voltage-controlled device can be stabilized in the negative-resistance region only when the source has a low impedance, and the device will be stable in either of the two states with a high-impedance source.

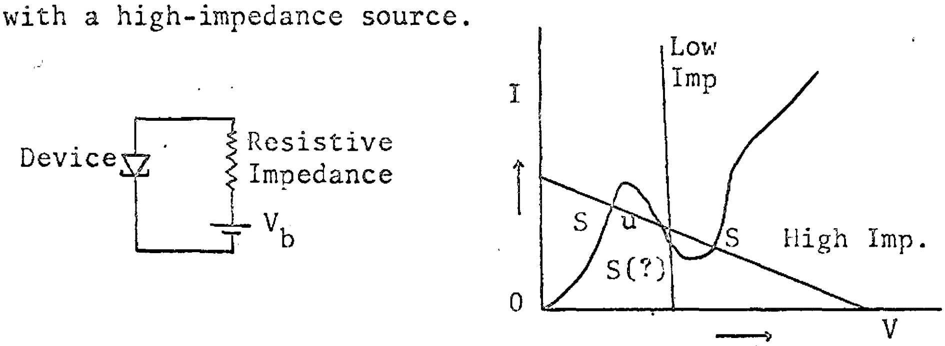

FIGURE 4.1: Tunnel Device and its Stability

Empirically, the circuit applications of a voltage-controlled device can broadly be divided into two groups, viz, (i) sinusoidal amplifiers and oscillators, or (ii) relaxation and switching circuits according as to whether the device is biased by a low- or high-impedance source.

There have been two publications so far in the literature; one by Giaever and Megerle[47] and the other by Miles, Smith and Schonbein[48] describing the attempts of using the superconducting tunnel diodes as active elements on the lines indicated above. Several similar experiments were conducted as a part of this thesis project to study the workability of tin-tin oxide-lead tunnel junctions, the fabrication of which is described in Section 2.3. Many limitations were encountered during these experiments and are discussed in detail in Chapter 5. Because of these limitations, the observations were confined to different types of oscillators and switching circuits.

4.2 Oscillators

The negative-conductance property of a tunnel diode makes it a convenient and desirable element for oscillators. Theoretically it may be made to oscillate at any frequency up to a few thousand Mhz, if the net conductance of the resultant tank circuit is negative[49]. To stabilize the frequency, a resonant circuit may be incorporated in the oscillator circuit. The resonant circuit is excited by the tunnel device and oscillates nearly at its resonant frequency, which in turn serves as a synchronizing signal to the device. The condition of oscillation for a resonant circuit coupled negative-resistance device requires that the total shunt conductance of the parallel resonant circuit or the total series resistance of the series resonant circuit be zero or negative.

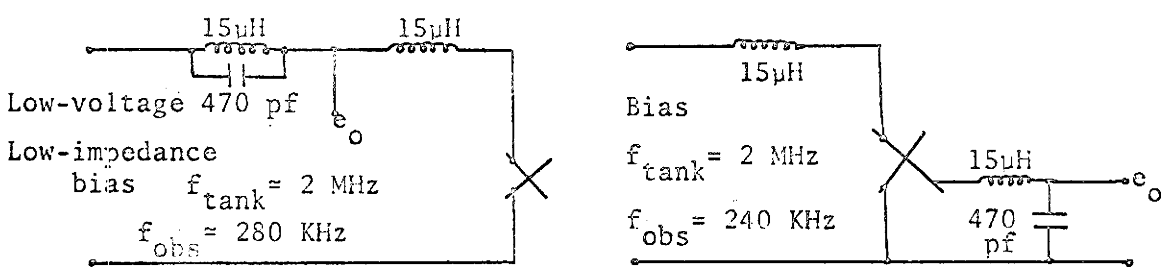

FIGURE 4.2: Two Types of Tuned Oscillators

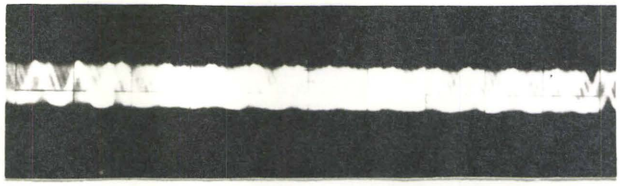

(a) Output of a tuned oscillator with series high impedance (Figure 5.2(a)
x-Sensitivity = 5 usec/div., y-Sensitivity = 200 uv/div.

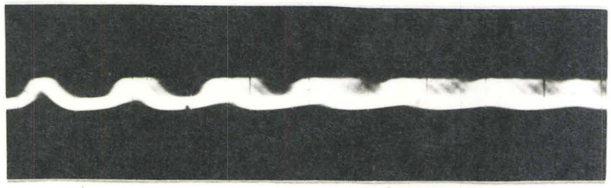

(b) Frequency of (a) is 'pulled' with a change (≈0.05mv) in bias voltage.
x-Sensitivity = 5 usec/div., y-Sensitivity = 200 uv/div.

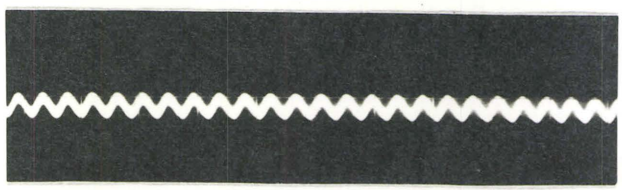

(c) Output of a tuned oscillator with parallel low impedance (Figure 4.2(b)
x-Sensitivity = 10 usec/div., y-Sensitivity = 200 uv/div.

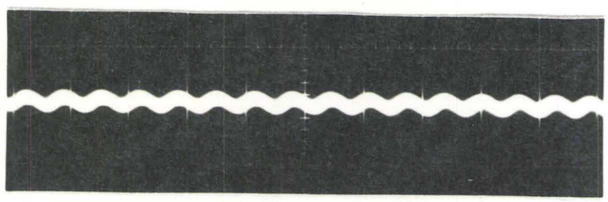

(d) Frequency of (c) is 'pulled' with a change (≈0.05mv) in bias voltage.
x-Sensitivity = 10usec/div., y-Sensitivity = 200 uv/div.

Figure 4.3 Oscilloscope traces of tuned oscillators (Figure 4.2)

The two circuits adopted for the superconducting tunnel junctions are shown in Figure 4.2. These were originally suggested by Ko[50] for the semiconducting tunnel diodes. If the Q of the resonant tank is high enough and also if the junction capacitance is not one of the principle resonant elements, it may be expected that the output waveform is sinusoidal and that the frequency is approximately the resonant frequency of the tank, without much dependence on the bias voltage. The waveforms shown in Figure 4.3, which are obtained from the circuits of Figure 4.2, are discuraging in view of the above expectation. It can be seen from Figure 4.3 the change in the frequency of oscillation with bias in both circuits is quite considerable and the tank resonance frequency and the observed frequency are widely different. These results show that the external tank capacitance is not large enough compared to the junction capacitance and that the frequency change with bias is probably due to the non-linearity of the negative-resistance region.

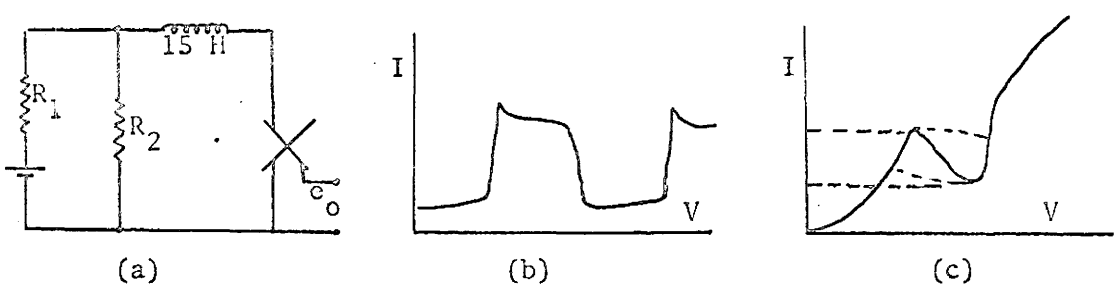

FIGURE 4.4: Relaxation Oscillator and Waveforms

When the total circuit inductance of a superconducting tunnel diode oscillator (Figure 4.4(a), with the diode biased in the negative-conductance region) is relatively large, the energy stored in this inductance due to flowing of current cannot be dissipated in a short period.

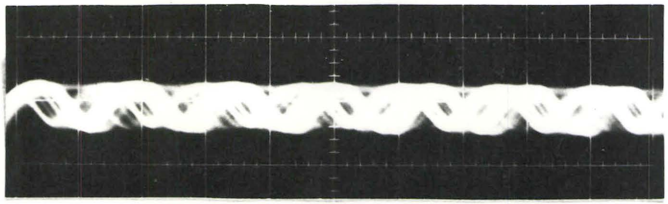

(a) Output of a relaxation oscillator (Figure 5.4(a).
x-Sensitivity = 5usec/div., y-Sensitivity = 200 uv/div.

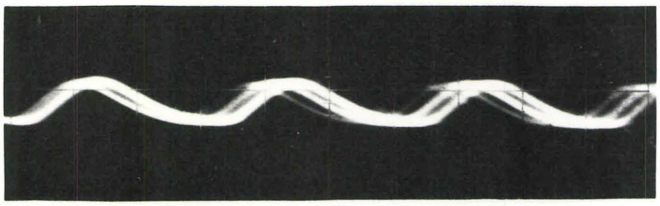

(b) Frequency of (a) is 'pushed' by a change in operating point.
x-Sensitivity = 2 usec/div., y-Sensitivity = 200 uv/div.

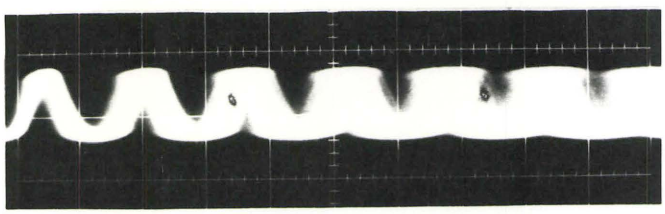

(c) Out put of a transmission-line oscillator (Figure 5.7(a)
x-Sensitivity = 5 usec/div., y-Sensitivity = 200 uv/div.

Figure 4.5 Oscilloscope traces of relaxation and transmission-line oscillators

The waveform approaches a square-wave shape (Figure 4.4(b)), because the excursion of the diode voltage is forced into the non-linear positive conductance regions (Figure 4.4(c)). This type of oscillation is referred to as a relaxation oscillation. However, since the lead and junction capacitances are of considerable magnitude, the rise and fall times are high enough that a triangular type of wave shape is observed experimentally, as shown in Figure 4.5(a) and (b). As in the previous case, the frequency is found to change with bias.

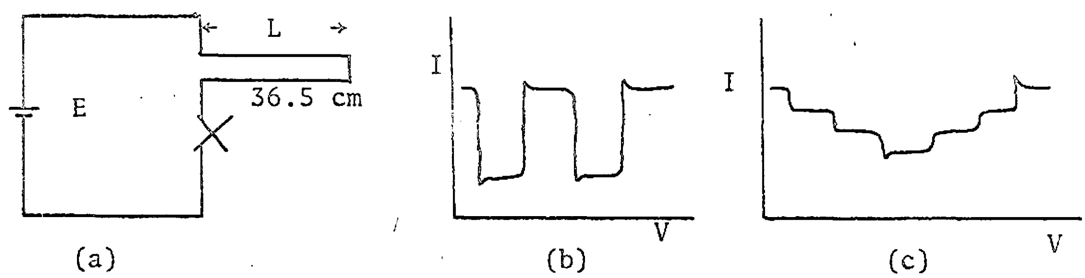

FIGURE 4.6: Transmission-line Oscillator and Waveforms

When a short-circuited coaxial cable, transmission line or artificial delay line is used, as shown in Figure 4.6(a), instead of the series inductance in the simple relaxation oscillator of the type described above, a good stable square wave is expected[51]. When the bias supply is switched on, the initial current determined by the bias voltage divided by the characteristic impedance of the cable and the diode resistance, propagates down the cable and reflects back because of the short circuit at the other end of the cable. The reflected current switches the diode into the high-voltage region. Since the bias voltage is smaller than the diode voltage in this region, the net voltage across the line is now reversed. A negative current pulse which passes down the cable is then reflected and switches the diode back into first region.

This process then repeats, as shown in Figure 4.6(b), with a period approximating to four times the period required for the electromagnetic wave to travel the length of the cable. However, when the characteristic impedance of the cable is large compared to the diode resistance, it requires more steps to build up and decay as shown in Figure 4.6(c). When the impedance becomes very large, the waveform approaches that of a relaxation oscillator. In an attempt to use a superconducting tunnel junction with a barrier resistance of about 1.6 Ω and a cable with a characteristic impedance of 50 Ω, this relaxation type of wave form was observed and is presented in Figure 4.5(c).

4.3 Switching Circuits

A tunnel diode, a battery and a resistor can be used to make a simple memory circuit. Figure 4.7 shows the circuit and a simple load line graph of its behaviour. The solid straight line is the I-V characteristic of the resistor and battery combination. If no input or output current is flowing, the diode may be at equilibrium with the circuit at points A, B or C. Point A, of course, corresponds to meta-stable equilibrium, and thus any perturbation would bring the operating point either to B or to C.

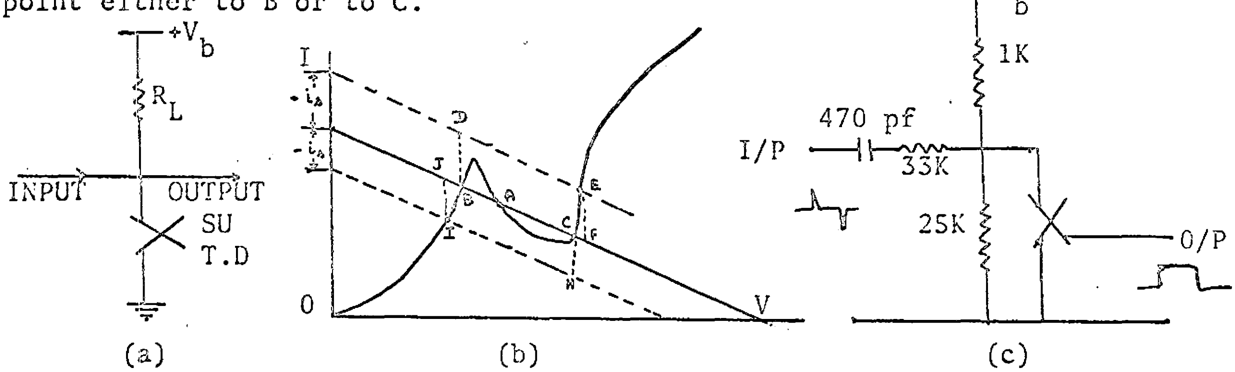

FIGURE 4.7: Bistable Circuits and I-V Trajectory

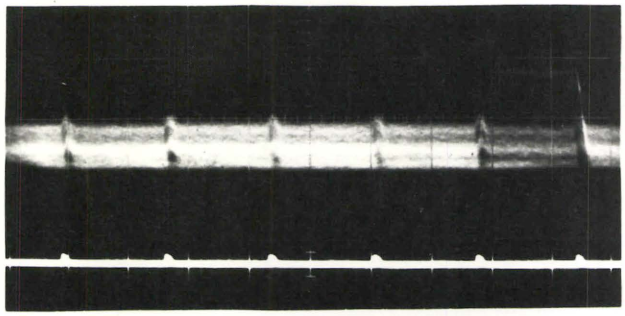

(a) Bistable Switching (upper beam). Trigger pulses (30kc/sec. Lower trace)
x-Sensitivity = 20 usec/div., Y_{UP}-Sensitivity = 200 uv/div., Y_{LO}-Sensitivity = 20mv/div.

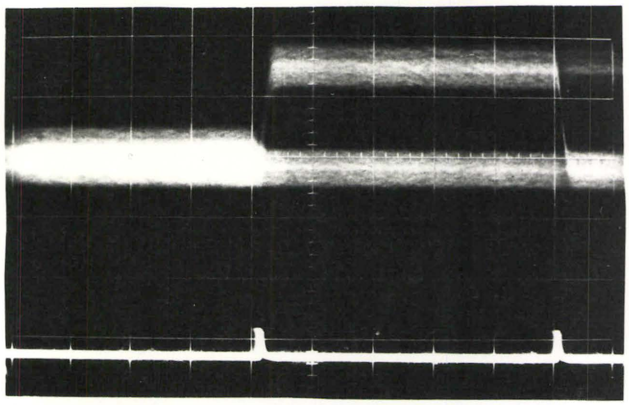

(b) Bistable Switching (upper beam). Trigger pulses (10 kc/sec. Lower beam)
x-Sensitivity = 20 usec/div., Y_{UP} -Sensitivity = 200 uv/div., Y_{LO} - Sensitivity = 20 mv/div.

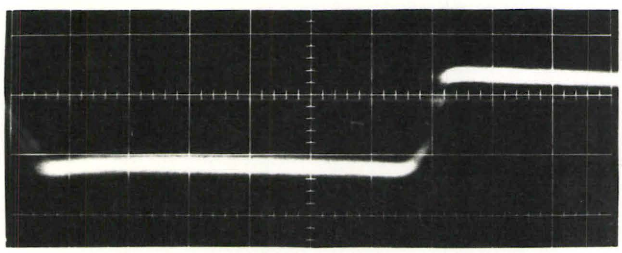

(c) Monostable Switching; high bias voltage
x-Sensitivity = 10 usec/div., Y-Sensitivity = 200 uv/div.

Figure 4.8 Oscilloscope traces of bistable and monostable operation

Let us assume that the circuit is initially quiescent and that the operating point is at B. If a trigger current $+i_s$ is temporarily injected, the operating point jumps instantaneously to point D and then the voltage rises with time as the junction capacitance charges. At E, a new quiescent point would be established, if the current i_s were to persist indefinitely. If i_s is removed, the operating point drops to F and then follows the trajectory FC. It will remain at C until a return to B is effected by applying a negative current $-i_s$ and removing it subsequently.

The circuit shown in Figure 4.7(c) is used to observe the bistable operation of a superconducting tunnel junction. This arrangement provides a variation in bias voltage by varying the relatively large supply voltage. Figures 4.8(a) and (b) show the waveforms obtained with triggering pulse frequencies of 30 KHz and 10 KHz, respectively. In both cases the negative pulses, $-i_s$, required to trigger the diode from the high-voltage region back to the low-voltage region are provided by the undershoots of these pulses (not seen on the traces because of the reduced sensitivity of 20 mV/div). The hazy appearance of the upper traces is due to pick-up noise which is probably from the unshielded leads running down the cryostat.

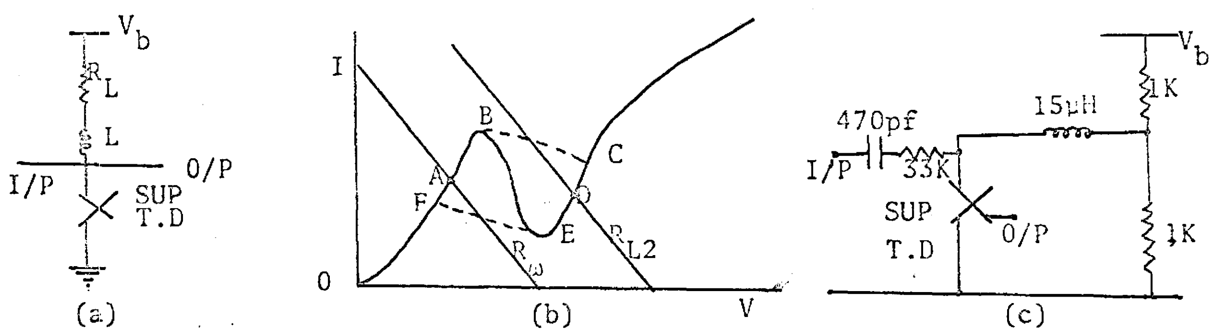

FIGURE 4.9: Monostable Circuits and I-V Trajectory

Another basic circuit tried with the superconducting tunnel diode is the monostable switch. This circuit will, when triggered from one state to the other, relax to the first state at some later time, dependent upon the circuit time constants. To establish one stable state a low resistance DC load line is required, and when it is triggered to the other semi-stable state a high AC impedance is provided by an inductor L connected as shown in Figure 4.9(a). The resistive load line is chosen to intersect the positive conductance sections of the characteristic as shown by R_{L1} and R_{L2} of Figure 4.9(b). If a load line such as R_{L1} is chosen, the quiescent point will be at A, and the circuit will be triggered by a positive pulse. In such a case the voltage across the diode increases momentarily to a magnitude corresponding to a point in the high-voltage region. This voltage swing or the voltage induced across the inductance can be taken as the output. R_{L2} has a quiescent point at D and will be triggered by a negative pulse. The output in this case is a negative voltage swing. The switching cycles for the two cases are therefore ABCDEFA and DEFABCD. The monostable circuit of Figure 4.9(c) may be used when a high voltage supply is available. The pulse output obtained from such a circuit with a superconducting tunnel junction biased in the high-voltage region is shown in Figure 4.8(c).

CHAPTER 5

SUMMARY AND CONCLUSIONS

An experimental and theoretical study has been made of superconductive tunneling in certain specific tunneling fabrications. Fabrication studies have been made of tin-lead, lead-lead and lead-alloy structures in which the insulating tunnel barrier has been thermally-grown oxide of the first-evaporated metal. The attendant difficulties of preparing such insulating barriers may limit the reliable use of such superconductive tunnel junctions as circuit application devices. Tunnel barriers of evaporated high dielectric strength materials might be used in place of the thermally-grown insulating barriers employed in this thesis. The evaporation of homogeneous insulator films of thickness in the order of 30 - 50 Å would however appear to be a difficult task, certainly as far as reproducability were concerned. Also better oxidation methods, such as anodization described by Miles and Smith[52], may be recommended for reproducable results.

The I-V characteristics of Sn/I/Pb superconductive fabrications as measured experimentally, have been compared with the theoretical characteristics as derived from a simple energy-gap model, analogous to that of a semiconductor. Although the semiconductor-gap analogy must be used with care when applied to the description of a superconductor, it is found that good agreement is obtained in the case of the Sn/I/Pb devices examined here.

Circuits have been designed and constructed to obtain the dI/dV and d^2I/dV^2 characteristics of such tunnel fabrications in a continuous form. In particular, the design of a 1 KHz narrow-band amplifier has been examined for use in such attendant circuitry. While the dI/dV characteristics of such devices yield information on the density-of-states of superconductors in question, the d^2I/dV^2 characteristics may be shown to yield information on the related phonon spectra. Analyses of these types may therefore yield information on the basic nature of the superconductive mechanisms in such materials. To avoid ambiguity in the interpretation of such density-of-states characteristics and of phonon spectra it is desirable to use symmetrical tunneling fabrications with the same superconductor on either side of the tunnel barrier. Such latter observations as made on Pb/I/Pb and Pb-alloy/I/Pb-alloy junctions from d^2I/dV^2 characteristics, were found to yield strong transverse and longitudinal phonon peaks near 4.4 mV and 8.4 mV corresponding to van Hove singularities. Further, as a result of low attainable modulation amplitudes, a good separation could be attained between the two transverse peaks at a temperature of 1.2^oK.

The Sn/I/Pb tunnel fabrication were examined as a potential superconductive circuit elements by virtue of their negative-resistance characteristics at liquid-helium temperatures. For such device applications as examined in this thesis it is to be noted that low-resistance barriers (1-10 Ω) are required. This limitation thus places some difficulties in the way of such device preparation. First, it is exceedingly difficult to produce such barriers without actually generating shorts between the superconductors forming the junction. Secondly, it was found that the lifetime of junctions successfully prepared was quite limited and usually ranged from a few hours to a day.

The use of these particular superconducting tunnel devices as amplifiers is not favourable because of the instabilities of the devices[53]. Further, and as a possible result of anisotropy in the energy gaps[34], the negative-conductance region of these devices was not a smooth one and the junction capacitance could not be obtained by direct measurements. Thus the performance of this tunnel junction as an amplifying device could not be reported in this thesis.

A brief study of different oscillator circuits was made and found to be discouraging from the same viewpoint of the nonlinear negative conductance. This resulted in a pronounced frequency shift for small bias changes as shown in Figure 4.3. It may be pointed out that for the case of the relaxation oscillator, since the I-V excursions would be around the negative-conductance region, a better frequency stability could be expected. However, the I-V characteristic is nonlinear outside the negative region as well[54], the effect of which is as presented in Figures 4.5(a) and (b), showing the frequency shift.

The transmission-line oscillator might have yielded a better result if a cable of low characteristic impedance has been employed. In the experiment reported in Section 4.2, however, a relatively high impedance ($Z_o = 50\ \Omega$) cable (compared to the sample resistance of $\sim 1.6\ \Omega$) resulted in a relaxation type of oscillation mode (Figure 4.5(c)).

The switching circuit applications of the tunnel device (Figure 4.8) would appear to be more promising if the pick-up noise due to the present system of connecting leads could be minimized. Integration of the total circuit on the same substrate[48] is suggested as a possible means of obtaining low-noise, high-frequency and high-speed operation.

REFERENCES

1. A. A. Abrikosov, Soviet Physics (USPEKHI), 8, 710 (1966).
2. H. K. Onnes, Phys. Lab. Univ. Leiden, No. 1196 (1911).
3. H. K. Onnes, Phys. Lab. Univ. Leiden, No. 1226 (1911).
4. F. B. Silsbee, J. Wash. Acd. Sci., 6, 597 (1916).
5. W. Meissner and R. Ochenfeld, Naturwissenschaften, 21, 787 (1933).
6. W. J. de Haas, and J. Voogd, Comm. Leiden, 214C (1931).
7. D. Shoenberg, Proc. Roy. Soc., A175, 49 (1940).
8. C. H. Gorter and H. B. G. Casimir, Phy. Z., 35, 963 (1934).
9. H. London and F. London, Proc. Roy. Soc., A149, 71 (1935).
10. K. Mendelssohn, Proc. Roy. Soc., A152, 34 (1935).
11. E. T. S. Appleyard, et al, Proc. Roy. Soc., A172, 540 (1939).
12. A. B. Pippard, Proc. Roy. Soc., A191, 385 (1947).
13. V. L. Ginzburg and L. D. Landu, J. Exp. Theo. Phys., 20, 1064 (1950).
14. N. V. Zavariskii, Doklady Akad. Nauk., 78, 665 (1951).
15. C. A. Reynolds, et al, Phy. Rev., 78, 487 (1950).
16. E. Maxwell, Phy. Rev., 78, 477 (1950).
17. H. Fröhlich, Phy. Rev., 79, 845 (1950).
18. J. Bardeen, Phy. Rev., 80, 567 (1951), Rev. Mod. Phys., 23, 261 (1951).
19. J. Bardeen, L. N. Cooper and J. R. Schrieffer, Phy. Rev., 108, 1175 (1957).
20. I. Giaever, Phy. Rev. Lets., 5, 147 (1960).

21. J. Nicol, S. Shapiro and P. H. Smith, Phy. Rev. Lets., 5, 461 (1960).

22. I. Giaever, Phy. Rev. Lets., 5, 464 (1960).

23. L. Esaki, Phy. Rev., 109, 603 (1958).

24. S. Shapiro, P. H. Smith, J. Nicol, J. L. Miles and P. F. Strong, IBM Jor., 6, 34 (1962).

25. L. C. Hebel, Phy. Rev., 116, 79 (1959).

26. I. Giaever, H. R. Hart and K. Megerle, Phy. Rev., 126, 941 (1962).

27. J. M. Rowell, A. G. Chynoweth and J. C. Phillips, Phy. Rev. Lets., 9, 59 (1962).

28. J. M. Rowell, P. W. Anderson and D. E. Thomas, Phy. Rev. Lets., 10, 334 (1963).

29. J. M. Rowell and L. Kopf, Phy. Rev., 137, A 907 (1965).

30. G. M. Eliashberg, Soviet Phys. JETP, 11, 696 (1960).

31. J. R. Schrieffer, D. J. Scalapino and J. W. Wilkins, Phy. Rev. Lets., 10, 336 (1963).

32. L. Van Hove, Phy. Rev., 89, 1189 (1953).

33. D. E. Thomas and J. M. Rowell, Rev. Sci. Insts., 36, 1301 (1965).

34. D. G. Walmsley, Ph.D. Thesis, McMaster University (1965).

35. R. C. Dynes, M.Sc. Thesis, McMaster University (1965).

36. B. T. Matthias, T. H. Geballe and V. B. Compton, Rev. Mod. Phys., 35, 1 (1963).

37. See e.g., Tanenbanm and Wright (Editors), "Superconductors" Interscience (1962).

38. R. W. Cohen, G. D. Cody and Y. Goldstein, RCA Rev., 25, 433 (1964).

39. D. A. Buck, Proc. IRE, 44, 482 (1956).

40. See e.g., N. S. Prywes (Editor) "Amplifiers and Memory Devices with Films and Diodes", McGraw-Hill (1965).

41. See e.g., H. R. Lowry, et al., "Tunnel Diode Manual", General Electric (1961).

42. R. Munoz, Electronic Design, 12, 56 (May 11, 1964).

43. T. G. Purnhagen, Electronics, 39, 88 (April 18, 1966).

44. R. J. Lamden, Electronic Engg., 35, 109 (1963).

45. G. Crisson, Bell Syst. Tech. Jor., 10, 485 (1931).

46. L. Esaki, Phy. Rev., 109, 603 (1958).

47. I. Giaever and K. Megerle, IRE Trans., ED-9, 459 (1962).

48. J. L. Miles, P. H. Smith and W. Schonbein, Proc. IEEE (corsp.), 51, 937 (1963).

49. See e.g., W. F. Chow, "Principles of Tunnel Diode Circuits", J. Wiley & Sons (1964).

50. W. H. Ko, Electronics, 34, 68 (Feb. 10, 1961).

51. M. C. Watkins, Electronic Design, 8, 54 (June 20, 1960).

52. J. L. Miles and P. H. Smith, J. Electrochemical Soc., 110, 1240 (1963).

53. J. Miles, Private Communication (July 18, 1966).

54. I. Giaever, Private Communication (Dec. 13, 1966).